JGR Biogeosciences

RESEARCH ARTICLE
10.1029/2022JG007106

Key Points:

- Downcore branched glycerol dialkyl glycerol tetraethers and alkenone measurements imply different magnitudes of Holocene air temperature variability on western Greenland
- Lake water temperatures during likely windows of biomarker production do not change at the same rate as air temperatures
- Lake water temperature-sensitive proxies are impacted by lake dynamics in seasonal environments

Supporting Information:

Supporting Information may be found in the online version of this article.

Correspondence to:

A. A. Cluett,
acluett@ucsc.edu

Citation:

Cluett, A. A., Thomas, E. K., McKay, N. P., Cowling, O. C., Castañeda, I. S., & Morrill, C. (2023). Lake dynamics modulate the air temperature variability recorded by sedimentary aquatic biomarkers: A Holocene case study from western Greenland. *Journal of Geophysical Research: Biogeosciences*, *128*, e2022JG007106. https://doi.org/10.1029/2022JG007106

Received 21 JUL 2022
Accepted 22 DEC 2022

Lake Dynamics Modulate the Air Temperature Variability Recorded by Sedimentary Aquatic Biomarkers: A Holocene Case Study From Western Greenland

A. A. Cluett[1,2], E. K. Thomas[2], N. P. McKay[1], O. C. Cowling[2], I. S. Castañeda[3], and C. Morrill[4]

[1]Institute of Marine Science, University of California Santa Cruz, Santa Cruz, CA, USA, [2]Environmental Research Division, NOAA Southwest Fisheries Science Center, Monterey, CA, USA, [3]Department of Geosciences, University of Massachusetts Amherst, Amherst, MA, USA, [4]Division of Paleoclimatology, NOAA National Center for Environmental Information, Boulder, CO, USA

Abstract Quantitative temperature reconstructions from lacustrine organic geochemical proxies including branched glycerol dialkyl glycerol tetraethers (brGDGTs) and alkenones provide key constraints on past continental climates. However, estimation of air temperatures from proxies can be impacted by non-stationarity in the relationships between seasonal air and water temperatures, a factor not yet examined in strongly seasonal high-latitude settings. We pair downcore analyses of brGDGTs and alkenones measured on the same samples through the Holocene with forward-modeled proxy values based on thermodynamic lake model simulations for a western Greenland lake. The measured brGDGT distributions suggest that stable autochthonous (aquatic) production overpowers allochthonous inputs for most samples, justifying the use of the lake model to interpret temperature-driven changes. Conventional calibration of alkenones (detected only after 5.5 thousand years BP) suggests substantially larger temperature variations than conventional calibration of brGDGTs. Comparison of proxy measurements to forward-modeled values suggests variations in brGDGT distributions monotonically reflect multi-decadal summer air temperatures changes, although the length of the ice-free season dampens the influence of air temperatures on water temperatures. Drivers of alkenone variability remain less clear; potential influences include small changes in the seasonality of proxy production or biases toward specific years, both underlain by non-linearity in water-air temperature sensitivity during relevant seasonal windows. We demonstrate that implied temperature variability can differ substantially between proxies because of differences in air-water temperature sensitivity during windows of proxy synthesis without necessitating threshold behavior in the lake or local climate, and recommend that future studies incorporate lake modeling to constrain this uncertainty.

Plain Language Summary Reconstructions of past temperature change from the Arctic are necessary to constrain long-term sensitivity of the region and the Greenland Ice Sheet to climate changes. We collected sediments from a western Greenland lake, which continuously accumulated for the past 9,000 years. In these sediments, we analyzed the chemical compositions of two temperature-sensitive classes of molecules produced by microorganisms within the lake. Surprisingly, the two proxies suggest different magnitudes of temperature changes when compared using conventional calibration approaches. Although changes in both proxies are often linked to air temperatures, they are likely more directly sensitive to water temperatures, which can differ from air temperatures—particularly in strongly seasonal environments like the Arctic. We use a lake model to simulate changes in lake water temperatures and convert to proxy units, enabling us to compare air and water temperatures to proxy measurements within a common frame of reference. We show that proxy sensitivity to air temperature changes can differ substantially depending on exactly when the proxies are produced. Because air and lake water temperatures during likely periods of production rarely change at the same rate, we suggest that future studies interpreting water temperature-sensitive proxies should incorporate lake modeling to constrain this uncertainty.

1. Introduction

As temperatures continue to rise in the Arctic (Davy et al., 2018), lakes across the region are undergoing physical changes including reductions in seasonal ice cover, increased water temperatures, and altered mixing regimes

(Mueller et al., 2009; Prowse et al., 2011; Saros et al., 2019; Woolway et al., 2020). Because even minor increases in air temperature can lengthen the duration of a lake's ice-free season (Palecki & Barry, 1986; Šmejkalová et al., 2016), high-latitude lakes are sensitive to climate changes and susceptible to climate-driven shifts in ecology and biogeochemical cycling (Luoto et al., 2019; Mueller et al., 2009; Prowse et al., 2011; Smol et al., 2005; Woelders et al., 2018), which then influence global climate via radiative and carbon cycle feedbacks (Bruhwiler et al., 2021; Kreplin et al., 2021).

Lake sediments preserve past terrestrial climate information, archiving paleotemperature proxies including branched glycerol dialkyl glycerol tetraethers (brGDGTs) and long-chain alkenones (Longo et al., 2018; Schouten et al., 2013). Quantitative temperature reconstructions from these and other organic geochemical proxies provide key constraints on past climate, but can be impacted by non-stationarity in proxy-temperature responses associated with biogeochemical and ecological changes within a lake and its catchment (Weber et al., 2018). For both proxies, changes in the microorganismal sources can modulate temperature-sensitivity and seasonality. For example, whether brGDGTs are produced primarily in the lake basin or in soils or where in the water column can vary in response to environmental changes (Tierney & Russell, 2009; van Bree et al., 2020; Weber et al., 2018). Similarly, alkenone-producing haptophyte species can be sensitive to changes in salinity and lake mixing regime (Longo et al., 2018; Theroux et al., 2020). Even more, non-stationarities resulting from proxy dynamics can be compounded by changes in the relationships between seasonal air and water temperatures (Cao et al., 2020; Dee et al., 2021), as lacustrine heat budgets are impacted by positive radiative feedbacks analogous to those operating at the Arctic-wide scale.

Proxy system models (PSMs), which simulate the proxy values expected for a prescribed climate state as translated stepwise through the proxy environment and sensor, can be used to quantitatively evaluate the sensitivity and seasonality of proxy responses to climate changes (Dee et al., 2015; Evans et al., 2013). In lacustrine systems, multi-proxy observations can be simulated from a common underlying lake model, with relevant aspects of the lake environment converted into specific proxy values using individual sensor models (Dee et al., 2018). By forward modeling proxy observations, PSMs enable quantification of the magnitude of proxy variability that can reasonably be explained by air and water temperature changes at different timescales. Moreover, simulation of the lake system including freezing and stratification processes enables consideration of potential non-linear or threshold behavior in lake and proxy responses to climate forcing.

The central western Greenland coast is the island's widest ice-free margin today, and therefore a region of interest for understanding past and present rates of ice sheet retreat (Briner et al., 2020). Across much of the Arctic, the Holocene (11.7 thousand years [ka] before 1950 CE to present) was characterized by several millennia of likely warmer-than-pre-industrial conditions followed by cooling in response to declining boreal summer insolation (Axford et al., 2021; Briner et al., 2016). On the central western Greenland coast, Holocene climate was influenced by freshwater forcing in the Labrador Sea and the proximity of the ice margin (Levy et al., 2018; Weiser et al., 2021; Young et al., 2020). However, the magnitude of these influences, which could have suppressed orbitally driven early Holocene warmth and modulated local ice sheet mass balance, remain poorly understood given the sparsity of quantitative local constraints on past temperature (Axford et al., 2021). No continental reconstructions from the region span the interval of highest boreal insolation due to the extent of the Greenland Ice Sheet at the time, leaving the local timing and magnitude of maximum Holocene temperature unresolved (Axford et al., 2021). Through the mid-to-late Holocene, existing temperature records disagree: summer temperature reconstructions based on alkenones measured in lake sediments from near the head of Kangerlussuaq Fjord indicate variations of up to 5.5°C over the past 5.6 ka (D'Andrea et al., 2011), whereas a chironomid-based reconstruction from North Lake near Ilulissat Fjord indicates cooling of only 2°C across the same interval (Axford et al., 2013). Determining whether differences between these reconstructions represent local variability in temperature or are driven by variations in proxy responses and resolution requires additional records from the region.

Here, we present two new temperature reconstructions from the sediments of one western Greenland lake using brGDGTs and alkenones. We then use a thermodynamic lake model to forward model proxy values under modern and perturbed climatological scenarios to evaluate the sensitivity of the lake environment and resulting proxy records to climate changes. The magnitude of reconstructed temperature variability differs substantially between the two proxies, despite their measurement within the same sediment samples. Forward modeling suggests that the proxies encode differing seasonal water-air temperature sensitivities, without necessitating threshold behavior in the lake system or local climate.

2. Background: Molecular Paleotemperature Proxies

2.1. Glycerol Dialkyl Glycerol Tetraethers

Glycerol dialkyl glycerol tetraethers (GDGTs) are microbial membrane lipids, typically present in lake sediments and soils (Schouten et al., 2013; Shanahan et al., 2013). Bacteria synthesize branched GDGTs (brGDGTs) with 15 commonly distinguished structures differentiated by number and position of cyclopentyl rings and methyl groups (Schouten et al., 2013; Sinninghe Damsté et al., 2018). The relative abundance of these brGDGT structures, commonly summarized by Methylation of Branched Tetraethers indices (De Jonge, Stadnitskaia, et al., 2014; Weijers et al., 2007), correlates with temperature, a relationship which has been demonstrated in mesocosm experiments, regional-to-global-scale lake sediment calibrations, and in situ monitoring of lake suspended particulate matter (SPM) (Loomis et al., 2014; Martínez-Sosa et al., 2021; Martínez-Sosa & Tierney, 2019; Miller et al., 2018; Raberg et al., 2021; Russell et al., 2018; Zhao et al., 2021). Following identification of distinct sets of brGDGT isomers with methyl groups in the 5 and 6 carbon positions, the most commonly reported brGDGT temperature-related index is MBT'_{5me}, which reflects changes among only 5-methyl isomers (De Jonge et al., 2013; De Jonge, Stadnitskaia, et al., 2014). In regions experiencing temperature seasonality, sedimentary lacustrine brGDGT distributions appear sensitive to warm-season temperatures rather than annual averages (Cao et al., 2020; Colcord et al., 2015; Keisling et al., 2017; Martínez-Sosa et al., 2021; Raberg et al., 2021; Shanahan et al., 2013; Sun et al., 2011; Zhao et al., 2021), and in the Arctic, measurements of downcore brGDGT relative abundances have been used to reconstruct past warm-season air temperature changes from the sediments of multiple lakes (e.g., Keisling et al., 2017; Lindberg et al., 2021; Thomas et al., 2018; Zhao et al., 2021).

The correlation of brGDGT distributions to temperature is likely the expression of a combination of homeoviscous membrane adaptations and bacterial community changes (De Jonge et al., 2019; Naafs et al., 2021). Because brGDGT distributions appear sensitive to their microbial sources, inferred variations in source communities due to changes in the contributions of aquatic and soil microorganisms or the development of distinct redox niches within a water column can complicate the inference of temperatures from brGDGT distributions (Kusch, Bennike, et al., 2019; Lattaud et al., 2021; Weber et al., 2018). Isoprenoid GDGTs (isoGDGTs) are a related set of compounds produced by Archaea, with 10 common structures distinguished by their degree of cyclization (0–8 cyclopentane rings) (Schouten et al., 2013). Production of isoGDGTs is linked to Archaea with methanogenic, methanotrophic, and non-methanogenic metabolisms that occupy separate niches within redox stratified lakes (Blaga et al., 2009; Schouten et al., 2013; Sinninghe Damsté et al., 2022). Although isoGDGTs are synthesized by different organisms than brGDGTs, community changes in isoGDGT-producing archaea can be associated with environmental changes that likely also influence bacterial brGDGT source organisms and communities (Blaga et al., 2009; Naeher et al., 2014; Weber et al., 2018; Wu et al., 2021; Z. Zhang et al., 2016).

2.2. Long-Chain Alkenones

Haptophyte algae synthesize long-chain alkenones, which are a class of methyl and ethyl ketones consisting of 35–42 carbons with two to four double bonds (D'Andrea et al., 2006; Longo et al., 2018). The relative abundance of double bonds among the C_{37} alkenones correlates to the water temperature in which they are synthesized, providing the foundation for use of the alkenone unsaturation index (U^K_{37}) to reconstruct sea surface and, more recently, lake water temperatures (Brassell et al., 1986; D'Andrea et al., 2016; Longo et al., 2016). Although alkenones are not ubiquitous in lake sediments, they are observed in the sediments and water columns of several high-latitude lakes (Harning et al., 2020; Longo et al., 2018; Richter et al., 2021), including oligosaline lakes (~1–3 practical salinity units [PSU]) near Kangerlussuaq, Greenland (D'Andrea & Huang, 2005). In low salinity (<5 PSU; the ocean is ~35.5 PSU) lakes, alkenone production is exclusively attributed to Group I haptophyte algae of the order Isochrysidales, which produce a distinct distribution of C_{37} alkenones with one abundant tetra-unsaturated homolog ($C_{37:4}$) and two tri-unsaturated isomers ($C_{37:3a}$ and $C_{37:3b}$) (Longo et al., 2016, 2018). In freshwater lakes containing alkenones, including those near Kangerlussuaq, the exclusive presence of Group I haptophytes in the modern water column has been confirmed by sequencing of environmental DNA (D'Andrea et al., 2006, 2016; Plancq et al., 2018; Richter et al., 2019; Theroux et al., 2010).

Modern observations of lake SPM and surface sediments suggest U^K_{37}-temperature sensitivity is constant across Group I species (D'Andrea et al., 2016; Longo et al., 2016), supporting the reconstruction of Holocene temperature variations based on downcore U^K_{37} variations in the sediments of freshwater Arctic lakes (D'Andrea

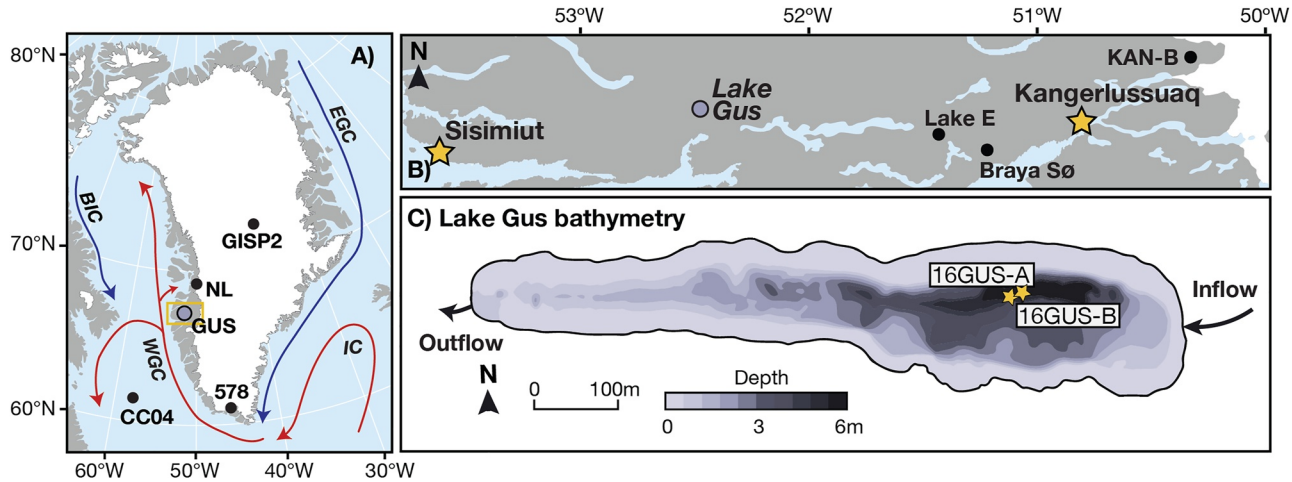

Figure 1. Maps of the study region. (a) Map of Greenland and modern Greenland Ice sheet extent (white) showing locations of inset map, Lake Gus (purple), and sites referenced in text: Lake 578 (Zhao et al., 2021), North Lake (Axford et al., 2013), ocean sediment core CC04 (Gibb et al., 2015), and the Greenland Ice Sheet Project 2 ice core (Kobashi et al., 2017). We show schematic surface ocean circulation: Irminger Current, East Greenland Current, West Greenland Current, and Baffin Island Current. (b) Map of study region including lakes from which alkenone records have been previously generated (Braya Sø and Lake E) (D'Andrea et al., 2006, 2011; D'Andrea & Huang, 2005), location of the KAN-B automatic weather station used to bias correct reanalysis data (Johansson et al., 2014), and locations of the towns of Sisimiut and Kangerlussuaq. (c) Bathymetric map of Lake Gus showing 16GUS-A and 16GUS-B core sites (stars).

et al., 2011, 2012; Harning et al., 2020; Longo et al., 2020; Richter et al., 2021; van der Bilt et al., 2018, 2019). For all currently published in situ Group I calibrations, U^{K}_{37}-temperature slopes are within error, albeit with different intercepts (D'Andrea et al., 2016; Longo et al., 2016, 2018). The site-specific seasonality of U^{K}_{37}-inferred temperatures is typically determined according to the seasonal temperatures controlling the timing and water temperatures of modern ice out and inferred haptophyte bloom, as sediment traps show highest alkenone fluxes early in the ice-free season during ice melt and isothermal mixing periods (D'Andrea et al., 2011, 2016; Longo et al., 2018). As a result, Arctic alkenone records have been interpreted to reflect winter/spring (Longo et al., 2020; Richter et al., 2021), early summer (D'Andrea et al., 2011), or average summer (JJA) temperature changes (D'Andrea et al., 2012; Harning et al., 2020; van der Bilt et al., 2018, 2019).

3. Methods

3.1. Site Description and Coring

Lake Gus (67.032°N, 52.427°W, 300 m above sea level; informal name) is a small (0.088 km^2, 6 m deep) seasonally through-flowing lake located approximately 90 km west of the modern Greenland Ice Sheet margin and 60 km north of Kangerlussuaq Fjord (Figure 1). Deglaciation of the 435 ha catchment occurred *c*. 10.4 ka (Young et al., 2020), yielding a narrow and relatively shallow basin (Figure 1c). Today, the catchment is vegetated with dwarf shrub tundra communities with abundant sedges and grasses. Among lakes in the Kangerlussuaq region, lake ice persists for up to 9 months a year, confining most hydrological and biological activity to a window within mid-June to October (Anderson & Brodersen, 2001; Johansson et al., 2014).

Near Lake Gus, summer moisture balance transitions from positive to negative along a gradient between the coast and the ice margin (Hasholt & Søgaard, 1978; Kopec et al., 2014). In July of 2016 and 2018, the lake was through-flowing with single small, channelized inflow and outflow streams. Similar water isotope values ($\delta^{18}O$ and $\delta^{2}H$) of the lake surface, inflow, and outflow indicated little catchment-wide evaporative isotopic enrichment, while similar $\delta^{18}O$ and $\delta^{2}H$ of the lake surface and bottom waters suggest the lake was well mixed (Cluett & Thomas, 2020). Most lakes in the region are dilute, except for closed-basin lakes near the head of the Kangerlussuaq Fjord (salinities of 1–3 PSU) (Anderson et al., 2001). On 7 August 2016, we collected surface sediment from one of these oligosaline lakes, Braya Sø (Figure 1b), from which high concentrations of alkenones have been reported (D'Andrea & Huang, 2005).

In July 2016, we collected three sediment cores from the depocenter of Lake Gus using a Universal Coring system. Prior to coring, we surveyed the lake's bathymetry with a Humminbird ONIX 10 Fishfinder and generated a bathymetric map using Autochart Live (Figure 1c). We then deployed the coring system from an inflatable raft

and pounded polycarbonate core tube into the sediment until refusal. We retrieved a 103-cm (16GUS-A1) and a 156-cm core (16GUS-A2) from core site A, and a 207-cm core (16GUS-B1) from core site B, both at 6 m water depth (Figure S1 in Supporting Information S1). Cores captured the undisturbed sediment-water interface, which we stabilized with Zorbitrol (Tomkins et al., 2008). After sitting vertically, core sediments compressed by approximately 40 cm, primarily due to water loss from the uppermost sediments and sections with visible mats of aquatic mosses. We drained any pooled water and packed all cores in the field, segmenting 16GUS-B1 in two (16GUS-B1b and 16GUS-B1a) for transport to the University at Buffalo (UB) Core Storage Facility (Buffalo, NY). At UB, we split the cores longitudinally and visually inspected and logged their stratigraphy. We stored all cores at 4°C.

3.2. Chronology

We developed a composite sequence of the 16GUS-A2 and 16GUS-B1 cores, aligning the two cores through comparison of stratigraphy and bulk sediment properties in Analyseries (Paillard et al., 1996) (Figure S1 in Supporting Information S1). In the composite sequence, composite depths of 158 cm and less are from 16GUS-B1 and those greater are from 16GUS-A2. We collected 11 samples of aquatic macrofossil fragments from 16GUS-A2 and 16GUS-B1 sediments (Table S1 in Supporting Information S1), which we rinsed with deionized water and freeze-dried. We targeted aquatic macrofossils to avoid terrestrial material, which can be preserved in permafrost prior to deposition in lake sediments and can yield anomalously old ages in Arctic lakes (Oswald et al., 2005), and because a hardwater effect is unlikely to strongly impact ages of aquatic macrofossils from small through-flowing lakes in the Kangerlussuaq region on crystalline bedrock (Bennike et al., 2010). We sent the macrofossil samples to the National Ocean Sciences Accelerator Mass Spectrometry Facility at the Woods Hole Oceanographic Institution for radiocarbon dating.

We developed an age-depth model in R using the rbacon package (Blaauw & Christen, 2011), based the age-depth model on the radiocarbon ages of the 10 aquatic macrofossils in the composite 16GUS-A2 and 16GUS-B1 core sequence (Figure S1 in Supporting Information S1). We set the section thickness at 5 cm, the mean accumulation rate of the prior at 50 years/cm (Figure S1c in Supporting Information S1), and assume the age of the surface is equivalent to the year in which we collected the core, 2016 CE (-66 ± 5 cal yr BP). We do not perform any reservoir correction, and calibrate radiocarbon ages to calendar years before 1950 CE (cal yr BP) using the IntCal20 Calibration curve (Reimer et al., 2020). We report all ages as the median with one sigma uncertainty.

We sub-sampled the cores for biomarker analyses in half-centimeter-thick increments spaced 1.0–8.0 cm apart, adjusted to obtain roughly 115-year resolution in our biomarker analyses, for 84 total biomarker sub-samples. We collected 92 additional half-centimeter-thick sub-samples for bulk sediment analysis (%C, %N, $\delta^{13}C$, and $\delta^{15}N$) at 0.5–4.5 cm spacing (See Text S1 in Supporting Information S1), for a mean resolution of 60 years and at higher resolution (*c*. 40 years) between 4.4 and 7.0 ka to confirm the alignment of cores through this interval. We collected all sub-samples from cleaned core faces and freeze-dried the sub-sampled sediments.

3.3. Biomarker Analysis

We followed established protocols to extract GDGTs and alkenones from sub-sampled sediments in the UB Organic and Stable Isotope Biogeochemistry Laboratory (Kim et al., 2010; Longo et al., 2018). See Text S2 in Supporting Information S1 for detailed laboratory methods for extraction, purification, and quantification. We calculate several established indices based on alkenone and GDGT relative abundances, including U^{K}_{37} and MBT'$_{5Me}$ (Table S2 in Supporting Information S1). We compare available MBT'$_{5Me}$ based lacustrine brGDGT-temperature calibrations, only excluding those of Dang et al. (2018), developed for alkaline lakes, and Harning et al. (2020), a site-specific cross-calibration between alkenone and brGDGT measurements, and in situ U^{K}_{37} based alkenone-temperature calibrations (Table S3 in Supporting Information S1). All indices and calibrations referred to in the text are defined in Tables S2 and S3 in Supporting Information S1, respectively. We performed principal component analysis (PCA) on brGDGT concentrations using the FactoMineR and Factoextra packages in R (Kassambara & Mundt, 2020; Lê et al., 2008). For PCA, we scaled brGDGT concentrations such that the most abundant brGDGT in each sample is assigned a value of 1.

3.4. U^{K}_{37} and MBT'$_{5Me}$ Forward Modeling

Our forward modeling approach relies on two steps: simulation of lake water temperatures under specified climate using the Hostetler and Bartlein lake energy and water balance model (Dee et al., 2018; Hostetler &

Bartlein, 1990) as adapted by Morrill et al. (2019) as the environment sub-model, and simulation of U^{K}_{37} and MBT'_{5Me} values from water temperatures at the relevant times of year using linear transfer functions as sensor sub-models (starred calibrations, Table S3 in Supporting Information S1).

3.4.1. Climate Forcing

We force PSM simulations with climate variables from the ERA5 Global Reanalysis Data set (Hersbach et al., 2020). We use 6-hourly ERA5 climate data from 1 January 1979 through 31 December 2019 at 0.1° latitude by 0.1° longitude resolution averaged over a box (66.9°–67.2°N, 50.1°–52.5°W) including the lake catchment and the KAN-B automatic weather station (AWS) (67.125°N, 50.183°W) (Johansson et al., 2014). We provide the model with surface forecast 2 m air temperature, 2 m dewpoint, 10 m windspeed, surface pressure, total precipitation, surface solar radiation downwards, and surface thermal radiation downwards at 6-hr timesteps. We estimate total precipitation for the 6-hr timestep by multiplying the hourly precipitation total by 6. We bias correct the ERA5 temperature, relative humidity, surface pressure, surface solar radiation downwards, and surface thermal radiation downwards with local instrumental climate data from the KAN-B AWS through quantile-quantile mapping, with separate quantile maps applied to the summer and winter seasons (Johansson et al., 2014; Morrill et al., 2019) (Figure S2 in Supporting Information S1). For perturbed temperature simulations, we uniformly increase and decrease annual and summer (JJAS) air temperatures in 0.5°C increments to ±10°C.

3.4.2. Lake Environment Sub-Model

We provide the lake model with bathymetric data in the form of depth-area slices at 1 m resolution (Figure 1c) and the area of the catchment calculated using the ArcHydro Toolbox in ArcGIS and the ArcticDEM (ESRI, 2017; Porter et al., 2018). We run the model on a 30-min time step for 31 model years, and a model sub-routine linearly interpolates each 6-hourly climate variable to 30-min time steps. We spin up the model through repetition of the first year of climate data (1979) 10 times, then save the daily fraction of lake ice cover, the mixing depth, and 1 m-resolution depth profiles of lake water temperature for the full 31 model years.

To constrain uncertainty associated with the model parameterization, we simulate Lake Gus under modern climate conditions with varied model parameters relevant to thermodynamic balance (snow albedo, slush albedo, shortwave extinction coefficient, neutral drag coefficient, sediment albedo, sediment conductivity, and sediment specific heat). We generate an ensemble of parameter values by simultaneously drawing from uniform distributions of each parameter 1,000 times using Latin Hypercube Sampling (Carnell & Carnell, 2016). We then run the model using each parameter set, and select the best performing parameter sets as those for which the median day of simulated lake ice break-up across model years occurs within the window of observed regional timing from 6 to 25 June (Anderson & Brodersen, 2001). We use the resulting best performing parameter sets as an ensemble for all modern and perturbed simulations, and report results as the mean and 95% high density intervals across ensemble members.

3.4.3. Sensor Sub-Models

To forward model MBT'_{5Me} and U^{K}_{37} from simulated lake water temperatures, we rely on linear transfer functions between temperature and proxy index values (See Table S3 in Supporting Information S1 for all calibration equations). We use the two MBT'_{5Me}-based transfer functions to convert simulated lake water temperatures to MBT'_{5Me} (Russell et al., 2018; Zhao et al., 2021). The in situ calibration of Zhao et al. (2021) (Z21), developed for a small southern Greenland lake, is the only available relevant calibration converting MBT'_{5Me} directly to water rather than air temperatures. The east African lakes calibration of Russell et al. (2018) was developed based on lakes spanning a non-seasonal low-latitude elevation transect, with MBT'_{5Me} calibrated to mean annual air temperature. Although the exclusive use of in situ water temperature-MBT'_{5Me} calibrations would be more appropriate, we are limited by the current availability of calibration data. Given the outstanding uncertainty in the exact seasonality of brGDGT production but evidence for a warm season bias (Cao et al., 2020; Deng et al., 2016; Stefanescu et al., 2021), we apply each calibration to multiple formulations of warm season-biased lake surface water temperature averages (i.e., June-August [JJA], months above freezing [MAF], and ice-free season), thus applying these calibrations to temperature seasonalities for which they are not explicitly calibrated. For U^{K}_{37}, we use available in situ calibrations for the Group I phylotype, which directly correlate U^{K}_{37} values to lake water temperatures (D'Andrea et al., 2011, 2016; Longo et al., 2018). We calculate U^{K}_{37} values based on lake water surface temperatures for possible alkenone production windows: the 2 weeks following ice-out, the isothermal mixing period, the full ice-free season, spring (MAM) and summer (JJA).

4. Results

4.1. Sedimentology and Chronology

The 156-cm-long 16GUS-A2 and 204-cm-long 16GUS-B1 cores consist of massive medium to dark brown gyttja, with abundant bryophyte macrofossils in the upper sediments and visually more clastic lower sediments (Figure S1 in Supporting Information S1). A thin mineral silt layer (approximately 1 mm thick) is present at core depths of 102 and 158 cm in 16GUS-B1 and 16GUS-A2, respectively, and corresponds to a peak in magnetic susceptibility and trough in Chl-*a* concentrations in both cores. Comparison of the stratigraphy, MS, and Chl-*a* between cores indicates that 16GUS-A2 contains a compressed sedimentary sequence relative to 16GUS-B1, supported by basal ages of 8,880 ± 110 cal yr BP for 16GUS-A2 and 4,880 ± 190 cal yr BP for the lowermost sediments in 16GUS-B1. The 10 aquatic macrofossils of the composite core sequence returned ages in stratigraphic order from 180 ± 150 to 8,880 ± 190 cal yr BP (Table S1 and Figure S1c in Supporting Information S1). All radiocarbon ages overlap with the 95% confidence interval of the age-depth model, which has a mean span of 514 years and ranges from 29 years at the core top to 1,435 years at 175 cm. Half-centimeter-thick biomarker samples represent between 5 and 70 years, with a mean duration of 20 years. For description of bulk sediment geochemistry, see Text S3 in Supporting Information S1.

4.2. Biomarkers

4.2.1. GDGTs

We identify branched and isoprenoid GDGTs in all analyzed Lake Gus sediment samples, with brGDGTs approximately one order of magnitude more abundant than isoGDGTs (Figure S3 in Supporting Information S1). Total brGDGT concentrations range from 2.1 to 6.5 ng g^{-1} dry sediment, and total isoGDGT concentrations range from 0.1 to 1.0 ng g^{-1} dry sediment. Total isoGDGT concentrations are highest and most variable in the early Holocene, and differ from changes in total brGDGT concentrations, which demonstrate comparatively consistent variability throughout most of the record (Figure S3 in Supporting Information S1).

The most abundant brGDGT in Lake Gus sediments is IIa (mean fractional abundance = 0.28 ± 0.03), followed by IIIa (0.26 ± 0.03), and Ia (0.25 ± 0.05) (Figure S3a in Supporting Information S1). Acyclic branched GDGTs (Ia, IIa, IIa', IIa, and IIIa'; 90% total) are more abundant than brGDGTs with one (8.1%) or two (1.1%) cyclopentane moieties, and 5-methyl isomers (83%) are more common than 6-methyl isomers (17%). As in other Arctic lake sediments, penta-methylated brGDGTs dominate (Lindberg et al., 2021; Raberg et al., 2021; Thomas et al., 2018; Zhao et al., 2021): 43% of measured brGDGTs are penta-methylated, while 31% and 26% are respectively hexa-methylated and tetra-methylated (Figure 2a, Figure S4a in Supporting Information S1).

In the PCA, most brGDGTs except for IIIa and IIa load positively on the first dimension (PC1), which explains 48.8% of variance (Figure 2b). Variations in PC1 scores are greater in the early than late Holocene (Figure S4b in Supporting Information S1). On the second dimension (PC2), which explains 13.5% of variance, Ic, Ib, IIIa, IIIa', and IIb' load positively while Ia and IIIb load negatively. Two clusters of samples emerge in the PC1-PC2 biplot, one trending from quadrant I to III and one in quadrant IV. The samples in quadrant IV are exclusively from the early Holocene and have low relative abundance of hexa-methylated brGDGTs. Comparison of sample coordinates on principal component and ternary axes consistently show two distinct clusters (Figures 2c–2h).

MBT'_{5Me}, HP_5, and *f*C demonstrate enhanced variability prior to *c*. 5.5 ka, and CBT_{5Me}, IR, and *f*C show defined first order trends following 5.5 ka (See Table S2 in Supporting Information S1 for all index definitions and equations; Figure 3, Figure S5 in Supporting Information S1) (De Jonge, Hopmans, et al., 2014; De Jonge, Stadnitskaia, et al., 2014; Martínez-Sosa & Tierney, 2019; Yao et al., 2020). Inferred temperatures are most variable in the early Holocene, then decline more steadily after 5 ka (Figure 3, Figure S6 in Supporting Information S1). Calibrated temperature anomalies are similar in magnitude across most calibrations. Absolute temperatures are within uncertainty among the Russell et al. (2018), Raberg et al. (2021), and BayMBT calibrations, but are approximately 5°C warmer with the Zhao et al. (2021) calibration (Table S3 in Supporting Information S1).

Caldarchaeol (GDGT-0) and crenarchaeol (GDGT-4) are the most abundant isoGDGTs, with mean fractional abundances of 0.79 ± 0.13 and 0.14 ± 0.12 (Figure S3b in Supporting Information S1), similar to sediments of other Arctic lakes (Daniels et al., 2021). Caldarchaeol is more abundant than crenarchaeol in all samples, although it decreases in absolute and relative abundances in step with an increase in crenarchaeol in the mid-Holocene. The

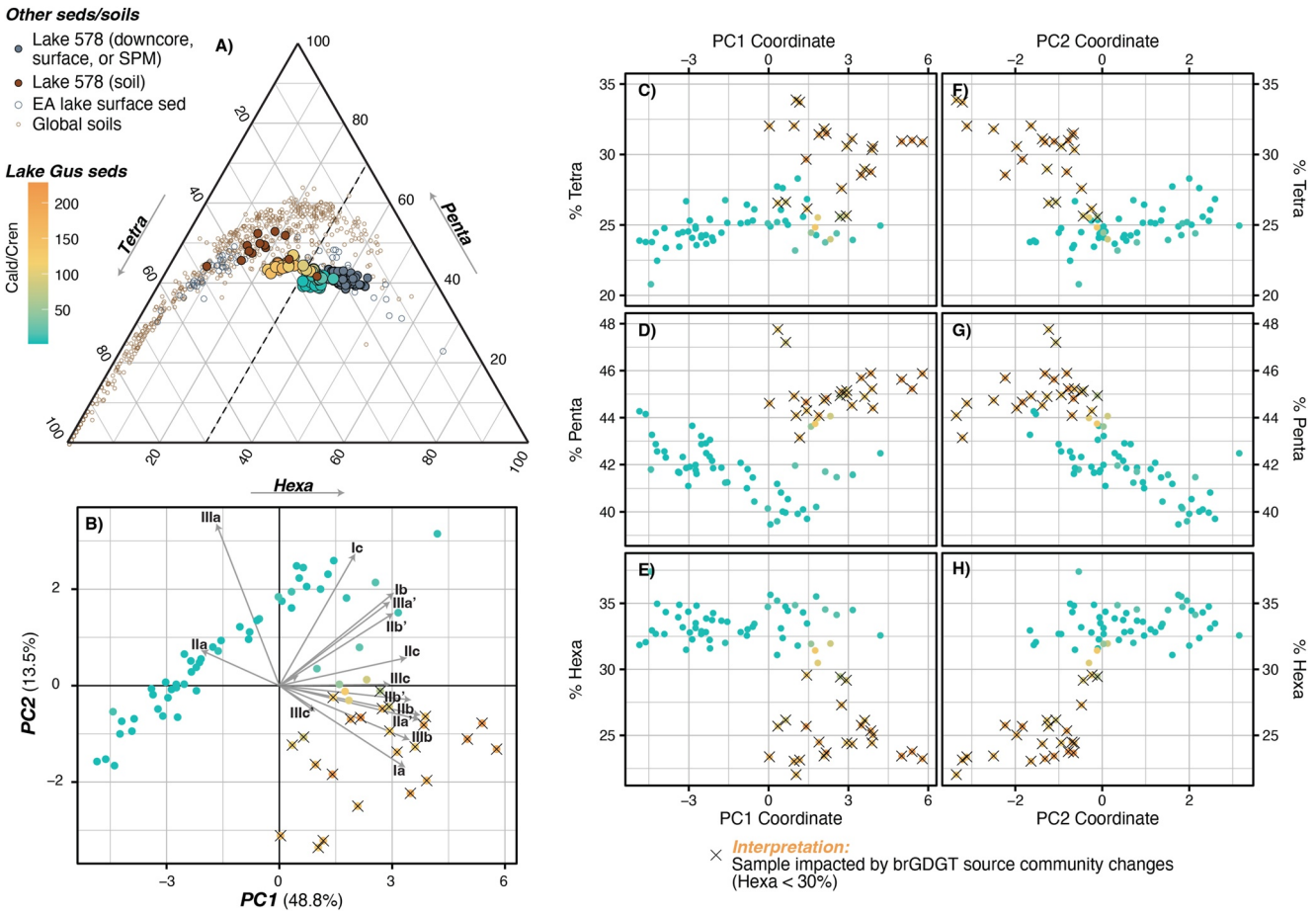

Figure 2. (a) Ternary diagram of the percentage of total tetra-, penta-, and hexa-methylated branched glycerol dialkyl glycerol tetraethers (brGDGTs) in Lake Gus sediments, in comparison to East African lake sediments (Russell et al., 2018), southern Greenland Lake 578 sediments and catchment soils (Zhao et al., 2021), and global soils (Dearing Crampton-Flood et al., 2020), as in figure legend. The dashed line marks 30% hexa-methylated brGDGTs. (b) Scaled brGDGT concentrations of Lake Gus samples on first and second principal component axes, including loadings of individual brGDGT compounds (arrows). (c–h) Lake Gus brGDGT samples on ternary and principal components axes. In all panels, Lake Gus samples are colored by the Cald/Cren ratio. In panels (b–h), samples with less than 30% hexa-methylated brGDGTs, which we interpret as being impacted by brGDGT source community changes, are marked by Xs.

ratio of caldarchaeol to crenarchaeol (Cald/Cren) ranges from 1.61 to 228 prior to stabilizing near a value of 2 *c*. 5.5 ka (Figure S5 in Supporting Information S1). GDGT-2, GDGT-3, and the crenarchaeol regioisomer (GDGT-4') occur in low fractional abundances, and were below the limit of quantification in several samples, preventing application of the TEX_{86} paleothermometer (Schouten et al., 2013).

4.2.2. Alkenones

The relative abundances of C_{37} alkenones were quantifiable in 18 of 83 samples (22%), first *c*. 5.5 ka and more consistently after 3.7 ka. In all samples that we quantify alkenones, we observe the full set of 16 alkenones characteristic of Group I haptophyte production from C_{37} to C_{39} (Figure S7 in Supporting Information S1). RIK_{37} varies from 0.51 to 0.57, consistent with the range for Group I Isochyrsidales of 0.48–0.63 (Longo et al., 2018), and U^K_{37} varies from −0.56 to −0.31 (Figure 3, Figure S6 in Supporting Information S1). There is some positive association between downcore U^K_{37} and RIK_{37} values ($R^2 = 0.244$, $p = 0.0037$). Previously observed similar small associations between RIK indices and temperature suggest that isomerization could be temperature-related, and that small isomerization changes are not necessarily indicative of haptophyte species changes (Longo et al., 2016). Reconstructed absolute temperatures differ among calibrations across a total range of 3.6–19.4°C, with individual calibrations spanning ranges of 8.6–11.7°C (Figure 3; Table S3 in Supporting Information S1).

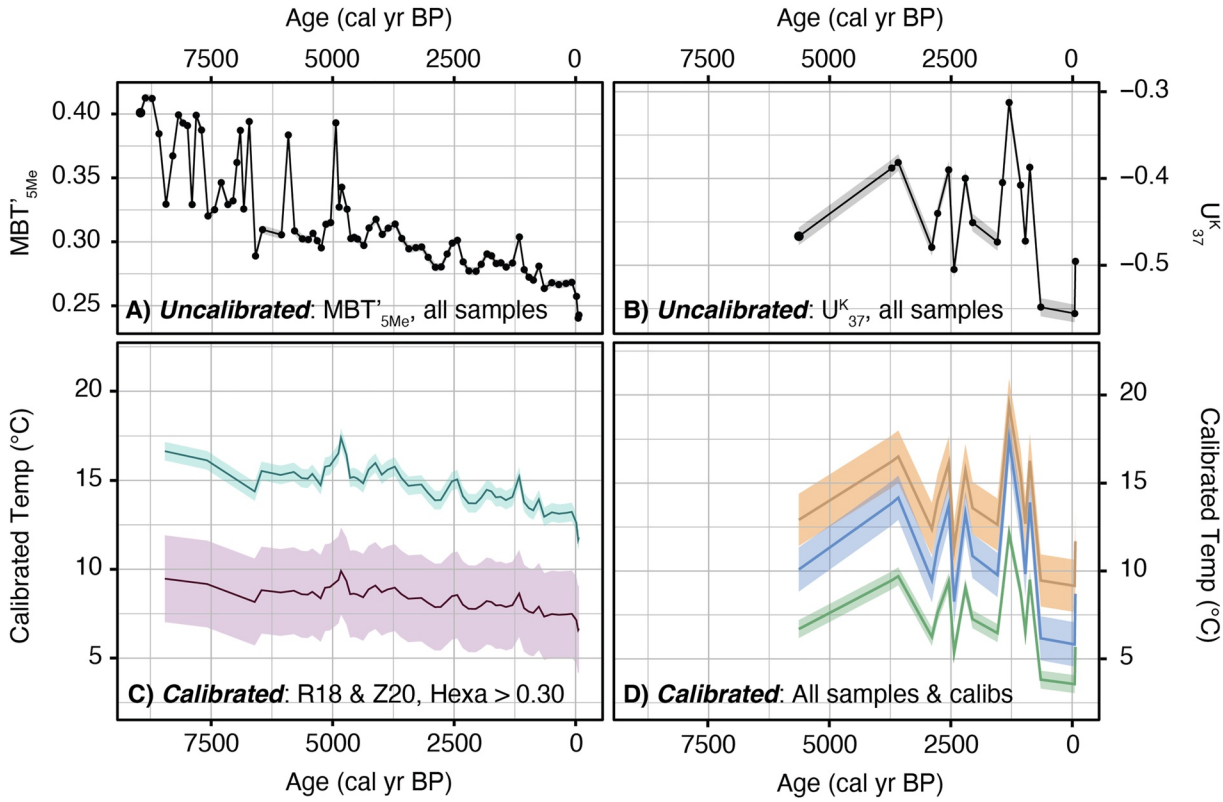

Figure 3. Branched glycerol dialkyl glycerol tetraethers (BrGDGT) and alkenone proxy records using a conventional inverse calibration approach. (a) Uncalibrated MBT'_{5Me} values for all measured samples. (b) Uncalibrated U^K_{37} values for all samples in which we detected alkenones. Gray error envelops denote analytical uncertainty determined from replicate samples. (c) Temperatures resulting from application of R18 (Russell et al., 2018; purple) and Z21 (Zhao et al., 2021; teal), R21 (Raberg et al., 2021; orange), BayMBT (dark blue) calibrations for branched glycerol dialkyl glycerol tetraether (brGDGT) samples with Hexa >0.30 (See Table S3 in Supporting Information S1 for calibration equations). (d) Temperatures resulting from R18 and Z21 calibrations for brGDGT samples with a fraction of hexa-methylated brGDGTs greater than 0.30. For temperatures resulting from other calibrations and for all brGDGT samples, see Figure S7 in Supporting Information S1.

4.3. Forward Modeling

4.3.1. Parameter Ensemble Selection

Of the 1,000 modern lake model simulations with varied parameter sets, 94 parameter sets yield a median date of lake ice melt within the observed regional timing (Figure S8 in Supporting Information S1). The albedo values of snow and slush and the neutral drag coefficient are significantly ($p < 0.001$) correlated to the date of lake ice melt, and the best performing parameter sets have low values of these parameters (Figures S8b, S8d, and S8e in Supporting Information S1). The light attenuation coefficient and specific heat, conductivity, and albedo of sediment are not significantly correlated to the timing of lake ice break up, and thus, the "best" parameter sets sample these values approximately uniformly across their ranges (Figures S8c and S8f–S8h in Supporting Information S1).

4.3.2. Simulation of Water Temperatures and Dynamics

The annual trajectory of lake water temperatures is similar across all simulations: the lake surface remains frozen throughout the winter and spring until surface temperatures quickly increase following ice melt in early to mid summer (June-August), prompting water column mixing (Figure S8a in Supporting Information S1). Surface water temperature increases rapidly following ice out, warming to near maximum summer temperature in one to 3 weeks and then stabilizing for up to 2 months, before cooling gradually and refreezing in mid-September. Among all parameter sets, the timing of ice melt and the rate of summer warming differ, while the rate of cooling in the fall and the timing of ice formation remain consistent, appearing insensitive to model parameterization (Figure S8a in Supporting Information S1).

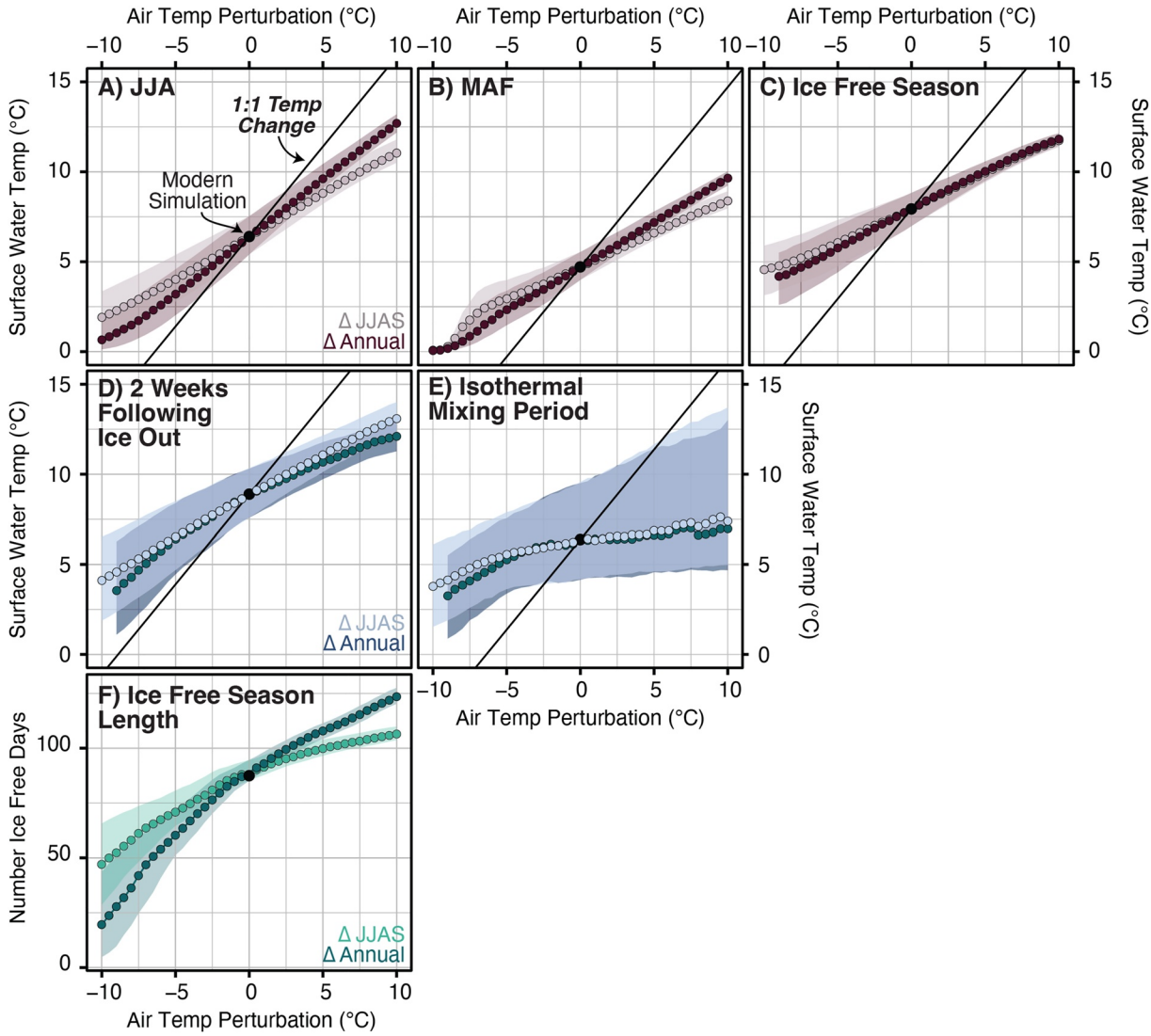

Figure 4. Sensitivity of lake water temperatures during specific seasonal windows (a–e) and the length of the ice-free season (f) to air temperature perturbations. Each point denotes the median value of the 40-year simulation average and error envelopes indicate the 95% confidence interval across the Proxy system model ensemble, for air temperatures changed during the summer only (light colors) or throughout the whole year (dark colors). Black points indicate the modern simulation, and lines indicate 1:1 temperature change (i.e., water temperatures change at the same rate as air temperatures).

In the perturbed lake model runs, changes in air temperature do not result in surface water temperature changes at the same rate. Although mean surface water temperatures during the summer (JJA), MAF, ice-free season, and 2 weeks following ice out increase monotonically with changes in air temperature (Figures 4a–4d), the relationships have a lower slope than 1:1, meaning that lake surface water temperatures change less than 1°C for every 1°C change in air temperature. Mean surface water temperatures during the isothermal mixing period, defined here as the period between the final break up of lake ice and the first day of partial water column stratification (mixing depth <5 m) show little sensitivity to increases in air temperature, with some non-monotonic behavior, and increased sensitivity to cooling of greater than 5°C (Figure 4e). Changes in surface water temperatures during these periods are similar when forced by summer and annual air temperature changes. The length of the ice-free season changes non-linearly in response to air temperature, with greater sensitivity to cooling below modern air temperatures and greater sensitivity to annual than summer air temperatures (Figure 4f).

4.3.3. Simulation of U^{K}_{37} and MBT'$_{5Me}$ Values

We reasonably simulate Lake Gus core top sediment U^{K}_{37} and MBT'$_{5Me}$ values, supporting the inferred windows of seasonal production and calibrations which make up the "sensor" sub-models (Figure 5). The uppermost core

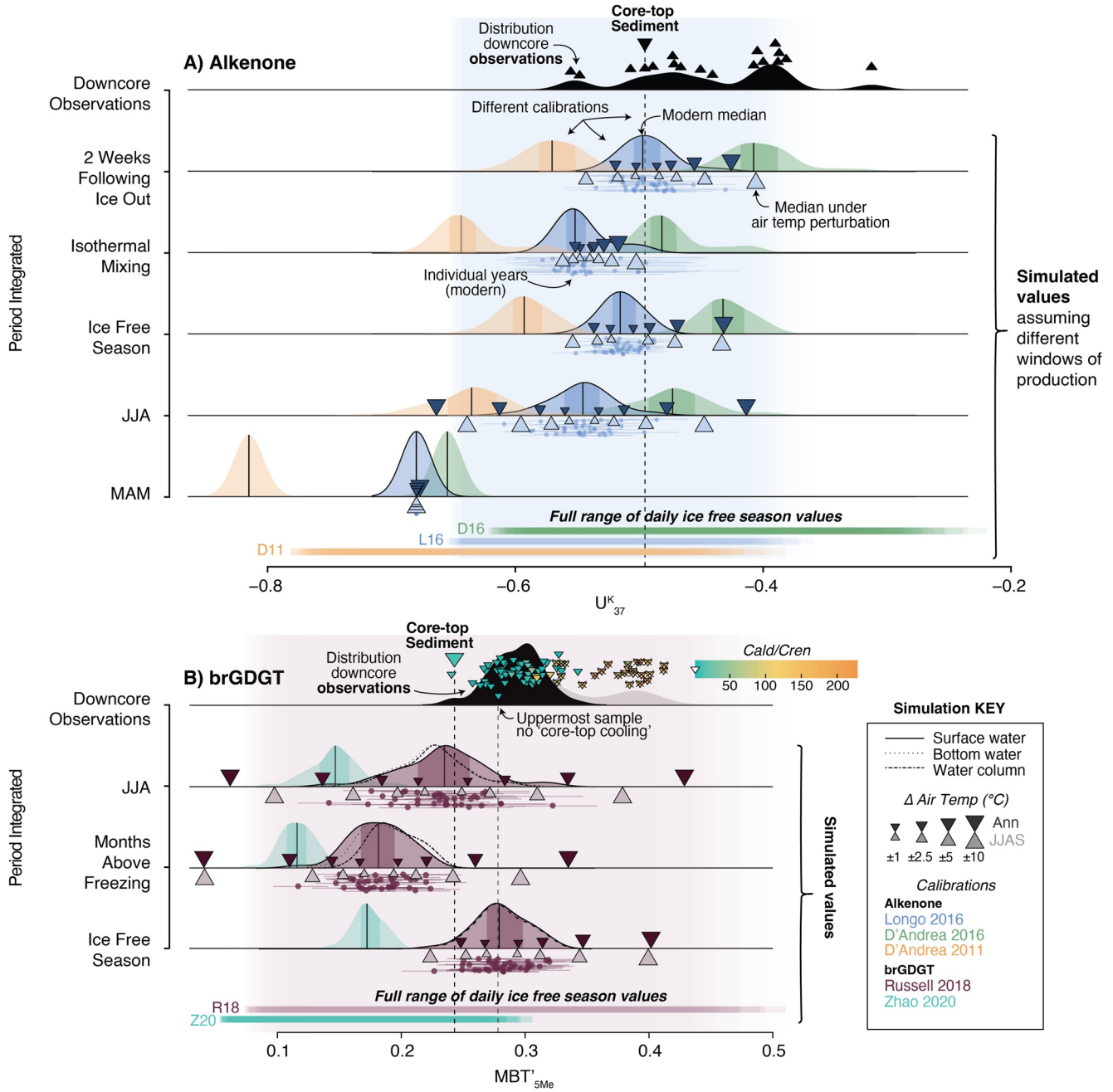

Figure 5. Forward modeled proxy values under modern and perturbed climate conditions for alkenone (a) and branched glycerol dialkyl glycerol tetraether (brGDGT) (b) indices. Black density distributions show the distribution of U^K_{37} and MBT'_{5Me} values (Hexa < 0.30; distribution for all MBT'_{5Me} values shown in gray), with triangle above showing individual sample values. For brGDGT samples, triangle color is determined by the Cald/Cren value of the sample, and samples which we interpret as being impacted by brGDGT source changes (Hexa < 0.30) are indicated by Xs. We note the value of the uppermost core sediment for each proxy, and also note the uppermost sample for brGDGTs which does not appear to be impacted by "core-top cooling." For simulated U^K_{37} and MBT'_{5Me} values assuming the windows of seasonal proxy production shown on the left axis, we show the density distributions of years within the 40-year modern simulation, with the center line showing the median value and the shaded region showing the interquartile range for each calibration (Table S3 in Supporting Information S1). Points below the density distributions show the values of individual years, with error bars representing the 95% confidence interval of the value across Proxy system model ensemble members, shown for best-fit calibrations only. Lines indicate the full range of daily ice-free season values for the modern simulation given each calibration. Triangles indicate the median values of perturbed simulations (i.e., multi-decadal median values) under prescribed changes to summer (JJAS) and annual air temperatures, which we would expect to be comparable to changes among downcore samples which integrate between 1 and 7 decades. Perturbed values are shown only for best-fit calibrations.

sediment has a U^K_{37} value of −0.50, equivalent to the median of the simulated 2 weeks following ice out calculated with the L16 calibration (Table S3 in Supporting Information S1). The surface sediment MBT'_{5Me} value of 0.24 is most closely approximated by the median JJA value calculated with the Russell et al., 2018 calibration (Table S3 in Supporting Information S1), although the uppermost sample which does not exhibit "core top cooling" (See discussion Section 4.1) most closely matches the median based on the ice-free season mean with the same calibration. Given their apparent best performance, we focus on the forward modeled values provided by the Longo et al. (2016) and Russell et al. (2018) calibrations throughout the discussion.

5. Discussion

The concentrations and distributions of alkenone and GDGT biomarkers measured in Lake Gus sediments are generally similar to those observed in other Arctic lake sediments (Harning et al., 2020; Lindberg et al., 2021). Yet, two puzzling features emerge when examining the multi-proxy record. First, brGDGT distributions demonstrate a shift in variability *c*. 5 ka apparent in most calculated indices (including MBT'_{5Me} and therefore inferred temperatures) and PCA (Figures 2 and 3, Figures S5–S7 in Supporting Information S1), coinciding with changes in isoGDGTs (Figure 2 and Figure S6 in Supporting Information S1) and our first detection of alkenones (Figure 3b). Second, in the Late Holocene, variations in U^K_{37}-inferred temperatures of 8–12°C in Lake Gus and of 5.5°C in the Kangerlussuaq-region records of D'Andrea et al. (2011) are substantially larger than estimates of summer air temperature from southern and western Greenland (~2°C) during the mid-late Holocene (Axford et al., 2021), including the brGDGTs which we measure within the same sediment samples here (Figure 3). Comparison of the two proxy records suggest that the magnitude of variability in one or both proxies does not reliably reflect the magnitude of local summer air temperature variability, at least for parts of the Holocene. Here, we evaluate the potential drivers of variability in MBT'_{5Me} and U^K_{37} as related to air temperature changes. For each proxy we use the forward-modeled framework to consider the explanatory potential of changes in the timescale being integrated, proxy seasonality, proxy-temperature non-stationarity, air-water temperature non-stationarity, and threshold behavior within the lake system. To support this approach, we first discuss evidence for brGDGT sources and the performance and limitations of the forward modeling approach. We then discuss the implications of inferred temperature changes in the context of other regional records and climate forcings.

5.1. Biomarker Source Attribution

The utility of forward modeling MBT'_{5Me} and U^K_{37} values using the lake PSM hinges on the establishment of a lacustrine source of the brGDGTs and alkenones in Lake Gus sediments—if the compounds are predominantly allochthonous, lake water temperatures would be irrelevant to their interpretation. While there is no evidence that alkenones are ever produced outside of lacustrine and marine settings (Theroux et al., 2010), brGDGTs occur in Arctic soils as well as lake water filtrates, SPM, and sediments (Harning et al., 2020; Kusch, Bennike, et al., 2019; Kusch, Winterfeld, et al., 2019; Peterse et al., 2014; Zhao et al., 2021), suggesting the potential for allochthonous or autochthonous production to contribute to the brGDGT pool archived in Lake Gus sediments. Previously, the BIT index (Figure S5 in Supporting Information S1) has been used to distinguish contributions of soil-derived brGDGTs from in situ production in nearshore marine sediments (Hopmans et al., 2004). However, conventional interpretation of the BIT index assumes all brGDGTs are produced in soils and is therefore not appropriate for discrimination of allochthonous and autochthonous brGDGTs in lake sediments (Castañeda & Schouten, 2011). Moreover, variations in BIT in Lake Gus sediments are mostly determined by changes in the concentration of crenarchaeol, which is not diagnostic of a specific source (Figure S5 in Supporting Information S1), as has been noted for other Arctic lakes (Daniels et al., 2021; Kusch, Bennike, et al., 2019). Instead, we rely on emergent differences between brGDGT distributions measured in soils and lake water filtrates, SPM, and sediments to discriminate between predominant autochthonous and allochthonous brGDGT production.

At a global scale, lake sediments generally contain more hexa-methylated and fewer tetra-methylated brGDGTs than soils (Naafs et al., 2017; Russell et al., 2018), which is evident in ternary space of the percentages of tetra-, penta-, and hexa-methylated brGDGTs (Figure 2a). In line with this pattern, the SPM, surface sediments, and downcore sediments measured from southern Greenland Lake 578 cluster near 20% tetra-methylated, 40% penta-methylated, and 40% hexa-methylated brGDGTs, distinct from its catchment soils, which generally have less than 25% hexa-methylated brGDGTs and overlap with the distribution of global soils (Naafs et al., 2017; Zhao et al., 2021). Most Lake Gus sediments cluster near SPM and sediments from Lake 578 (Southern Greenland, Zhao et al., 2021), which is consistent with a predominant in situ source of brGDGTs to the sediments of both lakes.

However, a subset of the oldest Lake Gus sediments plot between Lake 578 sediments and soils, with less than 30% hexa-methylated brGDGTs, which could indicate stronger soil contributions to this subset. Increased soil contributions during the earlier Holocene would be consistent with instability of the recently deglaciated landscape.

The Lake Gus samples with less than 30% hexa-methylated brGDGTs also generally have elevated ratios of caldarchaeol to crenarchaeol (Cald/Cren) and plot in quadrant IV of the PC1-PC2 biplot (Figure 2b). Caldarchaeol is abundant in association with methanogenic and methanotrophic Euryarchaeota (Pancost et al., 2001; Schouten et al., 2013), whereas crenarchaeol and its regioisomer (GDGT-4') are observed exclusively in cultures of Thaumarchaeota, which are limited to oxygenated waters (Schouten et al., 2013; Sinninghe Damsté et al., 2022; Stahl & de la Torre, 2012). Because of this redox-driven niche differentiation, Cald/Cren has been correlated to dissolved oxygen availability and used as an indicator of changing Archeal communities, stratification, and methane cycling in deep lakes (Blaga et al., 2009; Daniels et al., 2021; Qian et al., 2019; Y. G. Zhang et al., 2011; Z. Zhang et al., 2016). Elevated Cald/Cren in early Holocene samples could indicate a community shift from methanogenic to aerobic archaea driven by hypolimnetic oxygen depletion within the lake basin, which could be associated with a concurrent shift in brGDGT community influencing brGDGT distributions (Blaga et al., 2009). While it is tempting to interpret these changes as increased stratification during warmer summers of the early Holocene, lake model simulations indicate that persistent summer stratification is unlikely given the shallow depth and importance of wind-driven mixing in Lake Gus even under warmer air temperature scenarios (Figure S9 in Supporting Information S1). Alternatively, a combination of high summer productivity followed by a lengthened ice cover season during the heightened seasonality of the early Holocene could have strengthened respiration and oxygen drawdown under ice, resulting in winter-season anoxia as observed in some Arctic lakes today (MacIntyre et al., 2018). However, it is unclear the extent to which brGDGT production occurs under ice (Cao et al., 2020). Recent work indicates that inferred changes in brGDGT communities could occur without full anoxia (Stefanescu et al., 2021), or in response to micro-scale oxygen gradients (Halamka et al., 2021), raising the possibility that even subtle environmental changes could drive brGDGT source community changes.

Comparison of the coordinates of Lake Gus sediments along ternary and principal component axes consistently demonstrate that samples with low percentages of hexa-methylated brGDGTs, positive PC1 values and negative PC2 values, and high Cald/Cren form a distinct cluster (Figures 2c–2h). Taken together, these indicators suggest changes in brGDGT source community within the Early Holocene and into the Middle to Late Holocene, although it is unclear whether this is a shift from suboxic autochthonous production or allochthonous production to autochthonous oxygenated production. Determining whether distinct populations are the result of the relative importance of aquatic and soil sources, the influence of changing redox conditions within the lake and its sediments, or another factor influencing microbial communities remains challenging and should be a target of future research. Interestingly, the apparent shift in brGDGT source communities approximately coincides with our first detection of alkenones, potentially indicating a biogeochemical or ecological shift with impacts on both proxies.

Nonetheless, given the likelihood that source community changes overprint the influence of temperature in some brGDGT samples, we delineate the two populations by screening samples for those with less than 30% hexa-methylated brGDGTs (Figure 2a). This screening criteria identifies all samples that plot in the high MBT'_{5me} cluster as likely influenced by source community changes (Figure 5b). Similar options would be to screen the brGDGT samples based on PC scores or the Cald/Cren ratio. We favor use of the percentage of hexa-methylated brGDGTs for ease of comparison to brGDGT distributions from other soils and lake sediments, and note that each of these approaches would yield similar results here. Four samples with more that 30% hexa-methylated brGDGTs show somewhat high Cald/Cren and relatively low hexa-methylated brGDGTs, yet fall within the range of MBT'_{5Me} values among the other accepted samples. The observed GDGT distributions suggest that stable autochthonous (aquatic) production overpowers allochthonous inputs for most samples in the Middle to Late Holocene (those with less than 30% hexa-methylated brGDGTs), justifying the use of the lake model to interpret inferred temperature-driven changes in brGDGT distributions of those samples. However, we additionally caution against interpretation of the upper two samples in the screened brGDGT record that show evidence of "core top cooling," a phenomenon observed in several brGDGT records in which the uppermost core sediments appear to record artificially cold temperatures (Zhao et al., 2021).

5.2. Forward Modeling Validation and Uncertainties

The accuracy of forward modeled proxy values depends on the accuracy of simulated lake temperatures at relevant times, which depend on processes including freezing and mixing. The lake environment sub-model is configured

with known parameters (i.e., bathymetry) and harder-to-constrain parameters related to energy balance. These parameters are ideally calibrated through comparison of simulated lake water temperature timeseries to in situ temperature measurements over the historical period (Dee et al., 2018). However, collecting timeseries of temperature is not feasible from remote lakes visited once for the collection of a sediment core such as Lake Gus, which has been a repeated problem in application of this model in high-latitude settings. Whereas prior applications have adopted the parameters determined for other more well monitored lakes (Corcoran et al., 2021; Longo et al., 2020; Richter et al., 2021), we capitalize on the little regional observational data available, and develop an ensemble of model parameterizations.

We screen for the best performing ensemble members relative to the modern timing of ice out, based on field observations from multiple years (Anderson & Brodersen, 2001; Anderson et al., 1999; Lindborg et al., 2016). Whereas late summer and fall lake water temperatures are similar across all simulations, the parameterization impacts the timing of spring lake ice melt, rate of spring and early summer warming, and thus maximum summer lake water temperatures (Figure S8a in Supporting Information S1). Screening to the timing of ice out has the advantage of being a relatively easy piece of information to obtain via field observations or remote sensing, as well as providing constraint of lake behavior during periods relevant to the simulation of U^{K}_{37} and MBT'$_{5Me}$ values.

By generating an ensemble that samples the parameter space of poorly constrained parameters, which are unknown in the modern and could have changed in the past, we improve upon prior applications by more fully constraining parametric uncertainty. This should also help to avoid overfitting parameter values to modern conditions. Despite these uncertainties, we accurately simulate matches to core top sediment values for both U^{K}_{37} and MBT'$_{5Me}$ (Figure 5), and climate-driven changes in lake water temperatures and processes are smaller than the parametric uncertainty on climatically relevant scales (Figure 4).

5.3. Evaluation of U^{K}_{37} and MBT'$_{5Me}$ Variability in a Forward Modeled Framework

Comparison of downcore U^{K}_{37} and MBT'$_{5Me}$ observations to forward modeled values provides a quantitative framework for testing hypotheses regarding the mechanisms controlling downcore proxy variability (Figure 5). The simplest interpretations of these paleotemperature proxies generally rely on four assumptions: (a) equal production and preservation of biomarkers during all years recorded in a given sediment sample, (b) consistent seasonality of proxy synthesis, (c) stationary air-water temperature sensitivity within the relevant season, and (d) stationary biosynthetic proxy-temperature sensitivity. Within the framework of the PSM, we assess each of these assumptions, and discuss the likelihood of their influence on observed MBT'$_{5Me}$ and U^{K}_{37} values. Given the evidence for an overprinting effect of source community changes, we focus our analysis on the MBT'$_{5Me}$ values of samples with less than 30% hexa-methylated brGDGTs, as described in Section 4.1.

5.3.1. Assumption 1: Downcore Proxy Measurements Reflect Multi-Decadal Mean Temperatures

Based on the sedimentation rate in the Lake Gus cores, each half-cm thick sediment sample integrates between 5 and 70 years, with an average resolution *c*. 20 years (Figure S1 in Supporting Information S1). If we assume equal biomarker fluxes in all years, U^{K}_{37} and MBT'$_{5Me}$ values measured on homogenized sediment increments should represent the average of temperatures during the window of proxy seasonality for all years during which the sediment sample accumulated. This temporal integration would result in lower variability among measured sedimentary U^{K}_{37} and MBT'$_{5Me}$ than observed at interannual or, at high latitudes, intra-annual timescales. Downcore alkenone measurements span 0.25 U^{K}_{37} units. Assuming each observation represents a multi-decadal average, this magnitude of U^{K}_{37} change would necessitate sustained multi-decadal summer or annual air temperature changes of over 10°C. On the other hand, downcore MBT'$_{5Me}$ variations reasonably implicate multi-decadal summer or annual temperature changes up to approximately 5°C. The rejected MBT'$_{5Me}$ values, when taken separately from the rest of the data set, also span a reasonable range of multi-decadal variability, albeit at higher values. The unreasonably large multi-decadal variability in alkenones compared to GDGTs suggests that the assumption of equal production in all years is not valid for alkenones, although it may be for brGDGTs, presuming the other three assumptions are met.

The temperatures indicated by MBT'$_{5Me}$ and U^{K}_{37} values are inherently flux-weighted, dependent on the productivity of the source organisms. We only detect alkenones in a subset of downcore sediment samples from Lake Gus, indicating that their production is sporadic or varies substantially in magnitude between years. Intermittent production is supported by modern observations from other freshwater lakes which contain alkenones: in Braya

Sø, peak alkenone concentrations observed in the water column between two years differed substantially, at 15 in 2007 and 59 µg/L in 2009 (D'Andrea et al., 2011). Even more dramatically, across two summers for which Toolik Lake (N. Alaska) was monitored, peak alkenone fluxes captured in sediment traps differed by a factor of nearly 30 (Longo et al., 2018). It follows that on longer timescales, sedimentary U^K_{37} value would be biased toward the years with the greatest alkenone fluxes, and thus toward years or decades in which the timing of the haptophyte bloom coincides with favorable temperature, light, or nutrient conditions. While U^K_{37} values cannot reasonably be attributed to multi-decadal variability of a production during a specific seasonal window, it is possible that they are weighted toward a smaller subset of years and represent a selection of interannual variability under perturbed multi-decadal climate.

5.3.2. Assumption 2: Seasonal Windows of brGDGT and Alkenone Production Are Stable

Most downcore MBT'_{5Me} and U^K_{37} values fall within the total range of daily ice-free season values for a given calibration (Figure 5, bars along bottom of each proxy panel), indicating that changes in the seasonal production within the ice-free season could explain the observed values, even without any changes in climate. Sediment trap samples from Braya Sø revealed high alkenone fluxes in mid-June through mid-July, with particularly strong alkenone production in the 2 weeks following ice-out (D'Andrea et al., 2011). In Alaskan lakes, genomic biomarkers confirm the presence of Group I Isochrysidales haptophytes in the water column through periods of partial ice cover, isothermal mixing, and the onset of stratification in spring and summer (Richter et al., 2019), a transitional period across which the lake surface temperatures increased from 2 to 15°C (Longo et al., 2016, 2018). Because of these rapid changes in lake water temperature, which likely occur similarly in Lake Gus (Figure S8a in Supporting Information S1), even small shifts in the bloom timing could enhance magnitude of temperature variability recorded. MBT'_{5Me} values, which likely integrate temperatures across the warm season more fully, are less likely to be influenced by small changes in the seasonal timing of production.

5.3.3. Assumption 3: Air-Water Temperature Sensitivity Is Stationary During the Seasonal Windows of Alkenone and brGDGT Production

Lake surface water temperatures do not change 1:1 with air temperatures at multi-decadal timescales within any of seasonal windows that we consider, and most of these air-water temperature relationships show some amount of non-linearity (Figure 4). The variability in forced MBT'_{5Me} values is similar between all seasonal windows, although smaller for the ice-free season average than for MAF or JJA (Figure 5, triangles in middle panels). Generally, warm-season lake water temperatures increase linearly with warm-season and annual air temperatures, although the thermal inertia of the lake dampens the response of surface water temperature changes to air temperature changes as any heat gain is mixed down into the water column (Figures 4a–4c). This dampened sensitivity can also be explained by the dynamic length of the ice-free season, which changes non-linearly in response to air temperature (Figure 4f). With cooling, the duration of the ice-free season contracts, limiting the window during which water temperatures are impacted by air temperatures to the warmest part of the season. This suggests that MBT'_{5Me}-based temperatures are likely to be less variable than the air temperatures driving water temperature changes. However, we note that in our perturbed temperature scenarios we do not change the values of downward shortwave or longwave radiation, which would increase the incoming energy to the lake and stratification, and could shift the response of the surface water closer to the 1:1 line.

The variability in forced U^K_{37} values differs more substantially between seasonal windows than for the MBT'_{5Me} windows considered. For example, surface water temperatures during the isothermal mixing period (typically simulated as approximately 1 week following final ice break up) change minimally between years, limited to temperatures near freezing with a small impact of the rate of spring warming. If alkenones were produced exclusively during this period, we would expect them to record minimal water temperature changes. Interestingly, the temperature during the isothermal mixing period is the only non-monotonic air-water temperature relationship identified (Figure 4e), likely due to changes in the length of the mixing period. Yet, like the windows considered for MBT'_{5Me} values, water temperatures demonstrate reduced sensitivity to air temperature changes (Figures 4d and 4e), which we would expect to reduce variability in U^K_{37} values, opposite to our observations. Furthermore, we do not find evidence for thresholds except for with strong cooling, at which the ice-free season disappears in some years (Figure 4f).

5.3.4. Assumption 4: U^K_{37} and MBT'_{5Me}-Water Temperature Sensitivity Is Stationary

If sedimentary alkenones and brGDGTs in Lake Gus are consistently produced with stationary biosynthetic U^K_{37} and MBT'_{5Me}-water temperature sensitivity, we would expect one calibration to be able explain the observed

variability. U^{K}_{37}-temperature sensitivity varies according to the phylotype of alkenone-producing haptophyte, with phylotypes distinguished by salinity tolerance and distribution of alkenone compounds (D'Andrea et al., 2016). Group II and III phylotypes are restricted to brackish and saline lakes with salinity above 5 PSU (Crump et al., 2012; D'Andrea et al., 2016; Longo et al., 2016; Theroux et al., 2010). Lacking genetic data or salinity measurements from Lake Gus sediments, we rely on the RIK_{37} index as taxonomic indicator for Group I Isochrysidales, and RIK_{37} values of 0.52–0.57 are consistent with the values previously observed for Group I species (Longo et al., 2016). The oligosaline Kangerlussuaq lakes Braya Sø and Lake E, which are farther inland than Lake Gus (Figure 1b), are more strongly impacted by evapoconcentration, evident in solute and lake water isotope values, are thought to be dominated by Group I species (Theroux et al., 2012). If Lake E and Braya Sø remained dominated by Group I species throughout the Holocene, it is unlikely that Lake Gus would have been more susceptible to a shift to Type II species. There is phylogenetic diversity within Group I (Richter et al., 2019), and even if the U^{K}_{37}-temperature sensitivity was the same, differences in bloom timing as have been observed among Group II species could change U^{K}_{37}-air temperature sensitivity (Theroux et al., 2020). However, given the lack of genetic evidence that alkenone producing species shifted over the course of the record or that biosynthetic U^{K}_{37}-water temperature sensitivity varies among Group I species, this remains a purely speculative explanation for the observed U^{K}_{37} variability.

Although there is currently little information regarding exactly what organisms produce brGDGTs, the two populations of MBT'_{5Me} values in the full data set could indicate two different sources, each of which individually spans a reasonable range of temperature variability.

5.4. Summary of Possible Drivers of Proxy Variability and Interpretation of Climate Changes

The screened MBT'_{5Me} record (i.e., samples with fractional abundance of hexa-methylated brGDGTs <0.30) likely monotonically reflects multi-decadal summer air temperatures changes. However, given the relationship between water and air temperatures, conventional calibration of MBT'_{5Me} would likely underestimate the magnitude of local air temperature changes, which could misguide understanding of temperature-ice sheet sensitivity. The drivers of U^{K}_{37} variability remain less clear, with potential influences of small changes in the seasonality of proxy production or biases toward specific years amplifying proxy variability, underlain by non-linearity in water-air temperature sensitivity during windows of production which would likely work in the opposite direction. With these outstanding uncertainties in the proxy-air temperature relationships, we do not quantitatively interpret past temperature changes from the Lake Gus brGDGTs and alkenones, and instead compare uncalibrated proxy values to other regional quantitative temperature records.

MBT'_{5Me} declines from the early Holocene to present, indicating cooling following the trend in high-latitude summer insolation (Figures 6a and 6d). While the duration of terrestrial records from western Greenland are often limited by the extent of the Greenland Ice Sheet in the early Holocene, the warmest summer Labrador Sea surface temperatures of the Holocene are reconstructed prior to 6 ka (Gibb et al., 2015) (Figure 6g). These higher temperatures occurred toward the end of a period with some of the highest rates of Greenland Ice Sheet mass loss during the Holocene (Briner et al., 2020), when many mountain glaciers were smaller-than-modern (Schweinsberg et al., 2017, 2019), and after the Greenland Ice Sheet margin in the Kangerlussuaq region had retreated to near its late Holocene position (Lesnek et al., 2020). Although we do not clearly resolve temperature changes in the early Holocene here, the Lake Gus MBT'_{5Me} record suggests that shorter records may capture a local maximum in warmth c. 6–4 ka seen in Greenland Ice Sheet Project 2 temperatures (Figures 6b and 6c), but miss periods of earlier warmth c. 9.5–9 and 8–7 ka (Kobashi et al., 2017).

The transition from the middle to late Holocene was characterized by cooling and reduced strength of the West Greenland Current (Gibb et al., 2015; Moros et al., 2006; Perner et al., 2013), which could contribute to the millennial-scale cooling from early Holocene warmth apparent in the Lake Gus MBT'_{5Me} record. Yet, sub-millennial-scale variability in the Lake Gus brGDGT and alkenone records more closely resembles that of the Greenland Ice Sheet summit than that of summer temperatures in the Labrador Sea, such as the warming events c. 1.8 and 5 ka (Figures 6d–6g). An apparent link between temperatures on the Greenland Ice Sheet summit and the MBT'_{5Me} and U^{K}_{37} values measured here suggests sensitivity of western Greenland during the mid-to-late Holocene to large-scale atmospheric circulation, rather than local oceanographic conditions in the Labrador Sea or effects of the nearby ice sheet margin. Whereas sea surface temperature records from the Labrador Sea and Baffin Bay show strong site-to-site variability associated with shifting water masses (Axford et al., 2021),

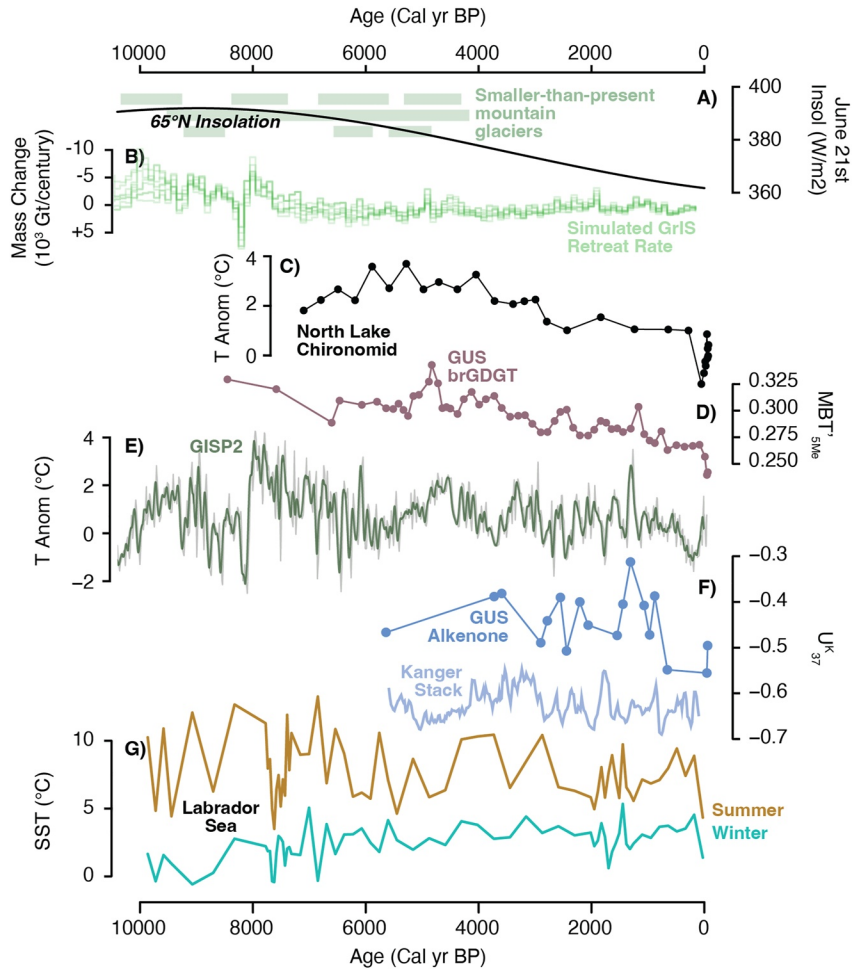

Figure 6. Holocene climate history from Lake Gus and western and central Greenland. (a) 21 June insolation at 65°N (Laskar et al., 2004) and periods of smaller-than-modern mountain glaciers on central western Greenland indicated by green boxes (Schweinsberg et al., 2017, 2019). (b) Simulated rates of Holocene Greenland Ice Sheet retreat given an ensemble of temperature and precipitation forcing scenarios (Briner et al., 2020). (c) Chironomid assemblage-inferred summer temperatures from North Lake (Figure 1a), (d) Uncalibrated branched glycerol dialkyl glycerol tetraether (brGDGT) MBT'_{5Me} values for samples with more than 30% hexa-methylated brGDGTs, this study. (e) Annual temperature anomalies inferred from gas fractionation from Greenland Ice Sheet Project 2 ice core (gray; Figure 1a)), with a 50-year running mean (green) (Kobashi et al., 2017). (f) Uncalibrated alkenone U^K_{37} values from this study and from the Kangerlussuaq-region stack (D'Andrea et al., 2011). (g) Summer and winter Labrador Sea surface temperatures (Figure 1a) (Gibb et al., 2015).

links between coastal and ice sheet temperature reconstructions would indicate a more homogenous terrestrial response. Changes in the dynamics of the ice-free season and alkenone production in Lake Gus likely impacted the magnitude of temperature changes suggested by the alkenones, without necessitating large changes in the local climate, and dampened the magnitude of temperature changes indicated by the brGDGTs. This suggests that the similar discrepancy in variability between previously published alkenone and chironomid-based temperature records from the region could be explained at least in part by differing impacts of lake water temperatures and dynamics on proxy responses, rather than strong local temperature heterogeneity. Non-linearity in lake water temperature responses become increasingly important as temperatures change from modern, and should be evaluated for lake water sensitive paleotemperature proxies prior to quantitively interpreting air temperature changes through the past.

Conflict of Interest

The authors declare no conflicts of interest relevant to this study.

Data Availability Statement

The proxy data reported in this study are available via the National Centers for Environmental Information (NCEI) paleoclimate database maintained by the National Oceanic and Atmospheric Administration (NOAA) at https://www.ncei.noaa.gov/access/paleo-search/study/38209. Lake model simulations are publicly archived on FigShare (https://doi.org/10.6084/m9.figshare.20353020), and code for analysis is available at: https://github.com/ACluett/Lake-Gus-Biomarkers.

Acknowledgments
We gratefully acknowledge the people of Kalaallit Nunaat. Funding for this research was provided by National Science Foundation (NSF) Grants ARCSS-1504267 and EAR IF-1652274 to EKT, and a University at Buffalo Department of Geology Champion Grant, the University at Buffalo Graduate Student Associated Mark Diamond Research Fund, Geological Society of America Graduate Student Research Grant, NSF Graduate Research Fellowship, and NSF-AGS Postdoctoral Research Fellowship 2114657 to AAC. We acknowledge field logistical support by CH2MHill Polar Field Services, and thank J. Briner, N. Young, H. Roop, and A. Lesnek for assistance in the field.

References

Anderson, N. J., Bennike, O., Christoffersen, K., Jeppesen, E., Markager, S., Miller, G., & Renberg, I. (1999). Limnological and palaeolimnological studies of lakes in south-western Greenland. *Geology of Greenland Survey Bulletin*, *183*, 68–74. https://doi.org/10.34194/ggub.v183.5207

Anderson, N. J., & Brodersen, K. P. (2001). Determining the date of ice-melt for low Arctic lakes along Søndre Strømfjord, southern West Greenland. *Geology of Greenland Survey Bulletin*, *189*, 54–59. https://doi.org/10.34194/ggub.v189.5156

Anderson, N. J., Harriman, R., Ryves, D. B., & Patrick, S. T. (2001). Dominant factors controlling variability in the ionic composition of West Greenland lakes. *Arctic Antarctic and Alpine Research*, *33*(4), 418–425. https://doi.org/10.1080/15230430.2001.12003450

Axford, Y., de Vernal, A., & Osterberg, E. C. (2021). Past warmth and its impacts during the Holocene thermal maximum in Greenland. *Annual Review of Earth and Planetary Sciences*, *49*(1), 279–307. https://doi.org/10.1146/annurev-earth-081420-063858

Axford, Y., Losee, S., Briner, J. P., Francis, D. R., Langdon, P. G., & Walker, I. R. (2013). Holocene temperature history at the western Greenland Ice Sheet margin reconstructed from lake sediments. *Quaternary Science Reviews*, *59*, 87–100. https://doi.org/10.1016/j.quascirev.2012.10.024

Bennike, O., Anderson, N. J., & McGowan, S. (2010). Holocene palaeoecology of southwest Greenland inferred from macrofossils in sediments of an oligosaline lake. *Journal of Paleolimnology*, *43*(4), 787–798. https://doi.org/10.1007/s10933-009-9368-x

Blaauw, M., & Christen, J. A. (2011). Flexible paleoclimate age-depth models using an autoregressive gamma process. *Bayesian Analysis*, *6*(3), 457–474. https://doi.org/10.1214/11-ba618

Blaga, C. I., Reichart, G.-J., Heiri, O., & Sinninghe Damsté, J. S. (2009). Tetraether membrane lipid distributions in water-column particulate matter and sediments: A study of 47 European lakes along a north–south transect. *Journal of Paleolimnology*, *41*(3), 523–540. https://doi.org/10.1007/s10933-008-9242-2

Brassell, S. C., Eglinton, G., Marlowe, I. T., Pflaumann, U., & Sarnthein, M. (1986). Molecular stratigraphy: A new tool for climatic assessment. *Nature*, *320*(6058), 129–133. https://doi.org/10.1038/320129a0

Briner, J. P., Cuzzone, J. K., Badgeley, J. A., Young, N. E., Steig, E. J., Morlighem, M., et al. (2020). Rate of mass loss from the Greenland Ice Sheet will exceed Holocene values this century. *Nature*, *586*(7827), 70–74. https://doi.org/10.1038/s41586-020-2742-6

Briner, J. P., McKay, N. P., Axford, Y., Bennike, O., Bradley, R. S., de Vernal, A., et al. (2016). Holocene climate change in Arctic Canada and Greenland. *Quaternary Science Reviews*, *147*, 340–364. https://doi.org/10.1016/j.quascirev.2016.02.010

Bruhwiler, L., Parmentier, F.-J. W., Crill, P., Leonard, M., & Palmer, P. I. (2021). The Arctic carbon cycle and its response to changing climate. *Current Climate Change Reports*, *7*(1), 14–34. https://doi.org/10.1007/s40641-020-00169-5

Cao, J., Rao, Z., Shi, F., & Jia, G. (2020). Ice formation on lake surfaces in winter causes warm-season bias of lacustrine brGDGT temperature estimates. *Biogeosciences*, *17*(9), 2521–2536. https://doi.org/10.5194/bg-17-2521-2020

Carnell, R., & Carnell, M. R. (2016). *Package 'lhs'*. CRAN. Retrieved from https://cran.rproject.org/web/packages/lhs/lhs.pdf

Castañeda, I. S., & Schouten, S. (2011). A review of molecular organic proxies for examining modern and ancient lacustrine environments. *Quaternary Science Reviews*, *30*(21–22), 2851–2891. https://doi.org/10.1016/j.quascirev.2011.07.009

Cluett, A. A., & Thomas, E. K. (2020). Resolving combined influences of inflow and evaporation on western Greenland lake water isotopes to inform paleoclimate inferences. *Journal of Paleolimnology*, *63*(4), 1–18. https://doi.org/10.1007/s10933-020-00114-4

Colcord, D. E., Cadieux, S. B., Brassell, S. C., Castañeda, I. S., Pratt, L. M., & White, J. R. (2015). Assessment of branched GDGTs as temperature proxies in sedimentary records from several small lakes in southwestern Greenland. *Organic Geochemistry*, *82*, 33–41. https://doi.org/10.1016/j.orggeochem.2015.02.005

Corcoran, M. C., Thomas, E. K., & Morrill, C. (2021). Using a paired chironomid $\delta^{18}O$ and aquatic leaf wax $\delta^{2}H$ approach to reconstruct seasonality on western Greenland during the Holocene. *Paleoceanography and Paleoclimatology*, *36*(4), e2020PA004169. https://doi.org/10.1029/2020pa004169

Crump, B. C., Amaral-Zettler, L. A., & Kling, G. W. (2012). Microbial diversity in arctic freshwaters is structured by inoculation of microbes from soils. *The ISME Journal*, *6*(9), 1629–1639. https://doi.org/10.1038/ismej.2012.9

D'Andrea, W. J., & Huang, Y. (2005). Long chain alkenones in Greenland lake sediments: Low $\delta^{13}C$ values and exceptional abundance. *Organic Geochemistry*, *36*(9), 1234–1241. https://doi.org/10.1016/j.orggeochem.2005.05.001

D'Andrea, W. J., Huang, Y., Fritz, S. C., & Anderson, N. J. (2011). Abrupt Holocene climate change as an important factor for human migration in West Greenland. *Proceedings of the National Academy of Sciences of the United States of America*, *108*(24), 9765–9769. https://doi.org/10.1073/pnas.1101708108

D'Andrea, W. J., Lage, M., Martiny, J. B., Laatsch, A. D., Amaral-Zettler, L. A., Sogin, M. L., & Huang, Y. (2006). Alkenone producers inferred from well-preserved 18S rDNA in Greenland lake sediments. *Journal of Geophysical Research*, *111*(G3), G03013. https://doi.org/10.1029/2005jg000121

D'Andrea, W. J., Theroux, S., Bradley, R. S., & Huang, X. (2016). Does phylogeny control U37K-temperature sensitivity? Implications for lacustrine alkenone paleothermometry. *Geochimica et Cosmochimica Acta*, *175*, 168–180. https://doi.org/10.1016/j.gca.2015.10.031

D'Andrea, W. J., Vaillencourt, D. A., Balascio, N. L., Werner, A., Roof, S. R., Retelle, M., & Bradley, R. S. (2012). Mild Little Ice Age and unprecedented recent warmth in an 1800 year lake sediment record from Svalbard. *Geology*, *40*(11), 1007–1010. https://doi.org/10.1130/G33365.1

Dang, X., Ding, W., Yang, H., Pancost, R. D., Naafs, B. D. A., Xue, J., et al. (2018). Different temperature dependence of the bacterial brGDGT isomers in 35 Chinese lake sediments compared to that in soils. *Organic Geochemistry*, *119*, 72–79. https://doi.org/10.1016/j.orggeochem.2018.02.008

Daniels, W. C., Castañeda, I. S., Salacup, J. M., Habicht, M. H., Lindberg, K. R., & Brigham-Grette, J. (2021). Archaeal lipids reveal climate-driven changes in microbial ecology at Lake El'gygytgyn (Far East Russia) during the Plio-Pleistocene. *Journal of Quaternary Science*, *37*(5), 900–914. https://doi.org/10.1002/jqs.3347

Davy, R., Chen, L., & Hanna, E. (2018). Arctic amplification metrics. *International Journal of Climatology*, *38*(12), 4384–4394. https://doi.org/10.1002/joc.5675

Dearing Crampton-Flood, E., Tierney, J. E., Peterse, F., Kirkels, F. M. S. A., & Sinninghe Damsté, J. S. (2020). BayMBT: A Bayesian calibration model for branched glycerol dialkyl glycerol tetraethers in soils and peats. *Geochimica et Cosmochimica Acta*, *268*, 142–159. https://doi.org/10.1016/j.gca.2019.09.043

Dee, S. G., Emile-Geay, J., Evans, M. N., Allam, A., Steig, E. J., & Thompson, D. M. (2015). PRYSM: An open-source framework for PRoxY System Modeling, with applications to oxygen-isotope systems. *Journal of Advances in Modeling Earth Systems*, *7*(3), 1220–1247. https://doi.org/10.1002/2015MS000447

Dee, S. G., Morrill, C., Kim, S. H., & Russell, J. M. (2021). Hot air, hot lakes, or both? Exploring mid-holocene African temperatures using proxy system modeling. *Journal of Geophysical Research: Atmospheres*, *126*(10), e2020JD033269. https://doi.org/10.1029/2020JD033269

Dee, S. G., Russell, J. M., Morrill, C., Chen, Z., & Neary, A. (2018). PRYSM v2.0: A proxy system model for lacustrine Archives. *Paleoceanography and Paleoclimatology*, *33*(11), 1250–1269. https://doi.org/10.1029/2018PA003413

De Jonge, C., Hopmans, E. C., Stadnitskaia, A., Rijpstra, W. I. C., Hofland, R., Tegelaar, E., & Damsté, J. S. S. (2013). Identification of novel penta-and hexamethylated branched glycerol dialkyl glycerol tetraethers in peat using HPLC–MS2, GC–MS and GC–SMB-MS. *Organic Geochemistry*, *54*, 78–82. https://doi.org/10.1016/j.orggeochem.2012.10.004

De Jonge, C., Hopmans, E. C., Zell, C. I., Kim, J.-H., Schouten, S., & Sinninghe Damsté, J. S. (2014). Occurrence and abundance of 6-methyl branched glycerol dialkyl glycerol tetraethers in soils: Implications for palaeoclimate reconstruction. *Geochimica et Cosmochimica Acta*, *141*, 97–112. https://doi.org/10.1016/j.gca.2014.06.013

De Jonge, C., Radujković, D., Sigurdsson, B. D., Weedon, J. T., Janssens, I., & Peterse, F. (2019). Lipid biomarker temperature proxy responds to abrupt shift in the bacterial community composition in geothermally heated soils. *Organic Geochemistry*, *137*, 103897. https://doi.org/10.1016/j.orggeochem.2019.07.006

De Jonge, C., Stadnitskaia, A., Hopmans, E. C., Cherkashov, G., Fedotov, A., & Sinninghe Damsté, J. S. (2014). In situ produced branched glycerol dialkyl glycerol tetraethers in suspended particulate matter from the Yenisei River, Eastern Siberia. *Geochimica et Cosmochimica Acta*, *125*, 476–491. https://doi.org/10.1016/j.gca.2013.10.031

Deng, L., Jia, G., Jin, C., & Li, S. (2016). Warm season bias of branched GDGT temperature estimates causes underestimation of altitudinal lapse rate. *Organic Geochemistry*, *96*, 11–17. https://doi.org/10.1016/j.orggeochem.2016.03.004

ESRI. (2017). *ArcGIS desktop: Release 10.5*. Environmental Systems Research Institute.

Evans, M. N., Tolwinski-Ward, S. E., Thompson, D. M., & Anchukaitis, K. J. (2013). Applications of proxy system modeling in high resolution paleoclimatology. *Quaternary Science Reviews*, *76*, 16–28. https://doi.org/10.1016/j.quascirev.2013.05.024

Gibb, O. T., Steinhauer, S., Fréchette, B., de Vernal, A., & Hillaire-Marcel, C. (2015). Diachronous evolution of sea surface conditions in the Labrador Sea and Baffin Bay since the last deglaciation. *The Holocene*, *25*(12), 1882–1897. https://doi.org/10.1177/0959683615591352

Halamka, T. A., McFarlin, J. M., Younkin, A. D., Depoy, J., Dildar, N., & Kopf, S. H. (2021). Oxygen limitation can trigger the production of branched GDGTs in culture. *Geochemical Perspectives Letters*, *19*, 36–39. https://doi.org/10.7185/geochemlet.2132

Harning, D. J., Curtin, L., Geirsdóttir, Á., D'Andrea, W. J., Miller, G. H., & Sepúlveda, J. (2020). Lipid biomarkers quantify Holocene summer temperature and ice cap sensitivity in Icelandic lakes. *Geophysical Research Letters*, *47*(3), e2019GL085728. https://doi.org/10.1029/2019GL085728

Hasholt, B., & Søgaard, H. (1978). Et forsøg på en klimatisk-hydrologisk regionsinddeling af Holsteinsborg Kommune (Sisimiut). *Geografisk Tidsskrift-Danish Journal of Geography*, *77*(1), 72–92. https://doi.org/10.1080/00167223.1978.10649095

Hersbach, H., Bell, B., Berrisford, P., Hirahara, S., Horányi, A., Muñoz-Sabater, J., et al. (2020). The ERA5 global reanalysis. *Quarterly Journal of the Royal Meteorological Society*, *146*(730), 1999–2049. https://doi.org/10.1002/qj.3803

Hopmans, E. C., Weijers, J. W., Schefuß, E., Herfort, L., Damsté, J. S. S., & Schouten, S. (2004). A novel proxy for terrestrial organic matter in sediments based on branched and isoprenoid tetraether lipids. *Earth and Planetary Science Letters*, *224*(1–2), 107–116. https://doi.org/10.1016/j.epsl.2004.05.012

Hostetler, S. W., & Bartlein, P. J. (1990). Simulation of lake evaporation with application to modeling lake level variations of Harney-Malheur Lake, Oregon. *Water Resources Research*, *26*(10), 2603–2612. https://doi.org/10.1029/WR026i010p02603

Johansson, E., Berglund, S., Lindborg, T., Petrone, J., van As, D., Gustafsson, L.-G., et al. (2014). Hydrological and meteorological investigations in a lake near Kangerlussuaq, west Greenland. *Earth System Science Data*, *7*(1), 93–108. https://doi.org/10.1594/PANGAEA.836178

Kassambara, A., & Mundt, F. (2020). Factoextra: Extract and visualize the results of multivariate data analyses. (R package v. 1.0. 5).

Keisling, B. A., Castañeda, I. S., & Brigham-Grette, J. (2017). Hydrological and temperature change in Arctic Siberia during the intensification of northern hemisphere glaciation. *Earth and Planetary Science Letters*, *457*, 136–148. https://doi.org/10.1016/j.epsl.2016.09.058

Kim, J.-H., Van der Meer, J., Schouten, S., Helmke, P., Willmott, V., Sangiorgi, F., et al. (2010). New indices and calibrations derived from the distribution of crenarchaeal isoprenoid tetraether lipids: Implications for past sea surface temperature reconstructions. *Geochimica et Cosmochimica Acta*, *74*(16), 4639–4654. https://doi.org/10.1016/j.gca.2010.05.027

Kobashi, T., Menviel, L., Jeltsch-Thömmes, A., Vinther, B. M., Box, J. E., Muscheler, R., et al. (2017). Volcanic influence on centennial to millennial Holocene Greenland temperature change. *Scientific Reports*, *7*(1), 1–10. https://doi.org/10.1038/s41598-017-01451-7

Kopec, B. G., Lauder, A. M., Posmentier, E. S., & Feng, X. (2014). The diel cycle of water vapor in west Greenland. *Journal of Geophysical Research: Atmospheres*, *119*(15), 9386–9399. https://doi.org/10.1002/2014jd021859

Kreplin, H. N., Santos Ferreira, C. S., Destouni, G., Keesstra, S. D., Salvati, L., & Kalantari, Z. (2021). Arctic wetland system dynamics under climate warming. *WIREs Water*, *8*(4), e1526. https://doi.org/10.1002/wat2.1526

Kusch, S., Bennike, O., Wagner, B., Lenz, M., Steffen, I., & Rethemeyer, J. (2019). Holocene environmental history in high-Arctic North Greenland revealed by a combined biomarker and macrofossil approach. *Boreas*, *48*(2), 273–286. https://doi.org/10.1111/bor.12377

Kusch, S., Winterfeld, M., Mollenhauer, G., Höfle, S. T., Schirrmeister, L., Schwamborn, G., & Rethemeyer, J. (2019). Glycerol dialkyl glycerol tetraethers (GDGTs) in high latitude Siberian permafrost: Diversity, environmental controls, and implications for proxy applications. *Organic Geochemistry*, *136*, 103888. https://doi.org/10.1016/j.orggeochem.2019.06.009

Laskar, J., Robutel, P., Joutel, F., Gastineau, M., Correia, A. C. M., & Levrard, B. (2004). A long-term numerical solution for the insolation quantities of the Earth. *Astronomy & Astrophysics*, *428*(1), 261–285. https://doi.org/10.1051/0004-6361:20041335

Lattaud, J., De Jonge, C., Pearson, A., Elling, F. J., & Eglinton, T. I. (2021). Microbial lipid signatures in Arctic deltaic sediments – Insights into methane cycling and climate variability. *Organic Geochemistry*, *157*, 104242. https://doi.org/10.1016/j.orggeochem.2021.104242

Lê, S., Josse, J., & Husson, F. (2008). FactoMineR: An R package for multivariate analysis. *Journal of Statistical Software*, *25*, 1–18. https://doi.org/10.18637/jss.v025.i01

Lesnek, A. J., Briner, J. P., Young, N. E., & Cuzzone, J. K. (2020). Maximum southwest Greenland Ice Sheet recession in the early Holocene. *Geophysical Research Letters*, *47*(1), e2019GL083164. https://doi.org/10.1029/2019GL083164

Levy, L. B., Kelly, M. A., Applegate, P. A., Howley, J. A., & Virginia, R. A. (2018). Middle to late Holocene chronology of the western margin of the Greenland Ice Sheet: A comparison with Holocene temperature and precipitation records. *Arctic Antarctic and Alpine Research*, *50*(1), S100004. https://doi.org/10.1080/15230430.2017.1414477

Lindberg, K. R., Daniels, W. C., Castañeda, I. S., & Brigham-Grette, J. (2021). Biomarker proxy records of Arctic climate change during the mid-pleistocene transition from Lake El'gygytgyn (far east Russia). Proxy Use-Development-Validation/Terrestrial Archives/Pleistocene. https://doi.org/10.5194/cp-2021-66

Lindborg, T., Rydberg, J., Tröjbom, M., Berglund, S., Johansson, E., Löfgren, A., et al. (2016). Biogeochemical data from terrestrial and aquatic ecosystems in a periglacial catchment, West Greenland. *Earth System Science Data*, *8*(2), 439–459. https://doi.org/10.5194/essd-8-439-2016

Longo, W. M., Huang, Y., Russell, J. M., Morrill, C., Daniels, W. C., Giblin, A. E., & Crowther, J. (2020). Insolation and greenhouse gases drove Holocene winter and spring warming in Arctic Alaska. *Quaternary Science Reviews*, *242*, 106438. https://doi.org/10.1016/j.quascirev.2020.106438

Longo, W. M., Huang, Y., Yao, Y., Zhao, J., Giblin, A. E., Wang, X., et al. (2018). Widespread occurrence of distinct alkenones from Group I haptophytes in freshwater lakes: Implications for paleotemperature and paleoenvironmental reconstructions. *Earth and Planetary Science Letters*, *492*, 239–250. https://doi.org/10.1016/j.epsl.2018.04.002

Longo, W. M., Theroux, S., Giblin, A. E., Zheng, Y., Dillon, J. T., & Huang, Y. (2016). Temperature calibration and phylogenetically distinct distributions for freshwater alkenones: Evidence from northern Alaskan lakes. *Geochimica et Cosmochimica Acta*, *180*, 177–196. https://doi.org/10.1016/j.gca.2016.02.019

Loomis, S. E., Russell, J. M., Heureux, A. M., D'Andrea, W. J., & Sinninghe Damsté, J. S. (2014). Seasonal variability of branched glycerol dialkyl glycerol tetraethers (brGDGTs) in a temperate lake system. *Geochimica et Cosmochimica Acta*, *144*, 173–187. https://doi.org/10.1016/j.gca.2014.08.027

Luoto, T. P., Rantala, M. V., Kivilä, E. H., Nevalainen, L., & Ojala, A. E. K. (2019). Biogeochemical cycling and ecological thresholds in a High Arctic lake (Svalbard). *Aquatic Sciences*, *81*(2), 34. https://doi.org/10.1007/s00027-019-0630-7

MacIntyre, S., Cortés, A., & Sadro, S. (2018). Sediment respiration drives circulation and production of CO_2 in ice-covered Alaskan Arctic lakes. *Limnology and Oceanography Letters*, *3*(3), 302–310. https://doi.org/10.1002/lol2.10083

Martínez-Sosa, P., & Tierney, J. E. (2019). Lacustrine brGDGT response to microcosm and mesocosm incubations. *Organic Geochemistry*, *127*, 12–22. https://doi.org/10.1016/j.orggeochem.2018.10.011

Martínez-Sosa, P., Tierney, J. E., Stefanescu, I. C., Dearing Crampton-Flood, E., Shuman, B. N., & Routson, C. (2021). A global Bayesian temperature calibration for lacustrine brGDGTs. *Geochimica et Cosmochimica Acta*, *305*, 87–105. https://doi.org/10.1016/j.gca.2021.04.038

Miller, D. R., Habicht, M. H., Keisling, B. A., Castañeda, I. S., & Bradley, R. S. (2018). A 900-year New England temperature reconstruction from in situ seasonally produced branched glycerol dialkyl glycerol tetraethers (brGDGTs). *Climate of the Past*, *14*(11), 1653–1667. https://doi.org/10.5194/cp-14-1653-2018

Moros, M., Jensen, K. G., & Kuijpers, A. (2006). Mid-to late-Holocene hydrological and climatic variability in Disko Bugt, central West Greenland. *The Holocene*, *16*(3), 357–367. https://doi.org/10.1191/0959683606hl933rp

Morrill, C., Meador, E., Livneh, B., Liefert, D. T., & Shuman, B. N. (2019). Quantitative model-data comparison of mid-Holocene lake-level change in the central Rocky Mountains. *Climate Dynamics*, *53*(1), 1077–1094. https://doi.org/10.1007/s00382-019-04633-3

Mueller, D. R., Van Hove, P., Antoniades, D., Jeffries, M. O., & Vincent, W. F. (2009). High Arctic lakes as sentinel ecosystems: Cascading regime shifts in climate, ice cover, and mixing. *Limnology and Oceanography*, *54*(6part2), 2371–2385. https://doi.org/10.4319/lo.2009.54.6_part_2.2371

Naafs, B. D. A., Gallego-Sala, A. V., Inglis, G. N., & Pancost, R. D. (2017). Refining the global branched glycerol dialkyl glycerol tetraether (brGDGT) soil temperature calibration. *Organic Geochemistry*, *106*, 48–56. https://doi.org/10.1016/j.orggeochem.2017.01.009

Naafs, B. D. A., Oliveira, A. S. F., & Mulholland, A. J. (2021). Molecular dynamics simulations support the hypothesis that the brGDGT paleothermometer is based on homeoviscous adaptation. *Geochimica et Cosmochimica Acta*, *312*, 44–56. https://doi.org/10.1016/j.gca.2021.07.034

Naeher, S., Peterse, F., Smittenberg, R. H., Niemann, H., Zigah, P. K., & Schubert, C. J. (2014). Sources of glycerol dialkyl glycerol tetraethers (GDGTs) in catchment soils, water column and sediments of Lake Rotsee (Switzerland) – Implications for the application of GDGT-based proxies for lakes. *Organic Geochemistry*, *66*, 164–173. https://doi.org/10.1016/j.orggeochem.2013.10.017

Oswald, W. W., Anderson, P. M., Brown, T. A., Brubaker, L. B., Hu, F. S., Lozhkin, A. V., et al. (2005). Effects of sample mass and macrofossil type on radiocarbon dating of arctic and boreal lake sediments. *The Holocene*, *15*(5), 758–767. https://doi.org/10.1191/0959683605hl849rr

Paillard, D., Labeyrie, L. D., & Yiou, P. (1996). AnalySeries 1.0: A Macintosh software for the analysis of geophysical time-series. *Eos*, *77*(39), 379. https://doi.org/10.1029/96eo00259

Palecki, M. A., & Barry, R. G. (1986). Freeze-up and break-up of lakes as an index of temperature changes during the transition seasons: A case study for Finland. *Journal of Applied Meteorology and Climatology*, *25*(7), 893–902. https://doi.org/10.1175/1520-0450(1986)025<0893:FUABUO>2.0.CO;2

Pancost, R. D., Hopmans, E. C., & Sinninghe Damsté, J. S. (2001). Archaeal lipids in Mediterranean cold seeps: Molecular proxies for anaerobic methane oxidation. *Geochimica et Cosmochimica Acta*, *65*(10), 1611–1627. https://doi.org/10.1016/S0016-7037(00)00562-7

Perner, K., Moros, M., Jennings, A., Lloyd, J., & Knudsen, K. (2013). Holocene palaeoceanographic evolution off West Greenland. *The Holocene*, *23*(3), 374–387. https://doi.org/10.1177/0959683612460785

Peterse, F., Vonk, J. E., Holmes, R. M., Giosan, L., Zimov, N., & Eglinton, T. I. (2014). Branched glycerol dialkyl glycerol tetraethers in Arctic lake sediments: Sources and implications for paleothermometry at high latitudes. *Journal of Geophysical Research: Biogeosciences*, *119*(8), 1738–1754. https://doi.org/10.1002/2014jg002639

Plancq, J., McColl, J. L., Bendle, J. A., Seki, O., Couto, J. M., Henderson, A. C. G., et al. (2018). Genomic identification of the long-chain alkenone producer in freshwater lake Toyoni, Japan: Implications for temperature reconstructions. *Organic Geochemistry*, *125*, 189–195. https://doi.org/10.1016/j.orggeochem.2018.09.011

Porter, C., Morin, P., Howat, I., Noh, M. J., Bates, B., Peterman, K., et al. (2018). *ArcticDEM, version 3*. Harvard Dataverse, V1. https://doi.org/10.7910/DVN/OHHUKH

Prowse, T., Alfredsen, K., Beltaos, S., Bonsal, B., Duguay, C., Korhola, A., et al. (2011). Past and future changes in Arctic lake and river ice. *AMBIO*, *40*(1), 53–62. https://doi.org/10.1007/s13280-011-0216-7

Qian, S., Yang, H., Dong, C., Wang, Y., Wu, J., Pei, H., et al. (2019). Rapid response of fossil tetraether lipids in lake sediments to seasonal environmental variables in a shallow lake in central China: Implications for the use of tetraether-based proxies. *Organic Geochemistry*, *128*, 108–121. https://doi.org/10.1016/j.orggeochem.2018.12.007

Raberg, J. H., Harning, D. J., Crump, S. E., de Wet, G., Blumm, A., Kopf, S., et al. (2021). Revised fractional abundances and warm-season temperatures substantially improve brGDGT calibrations in lake sediments. *Biogeosciences*, *18*(12), 3579–3603. https://doi.org/10.5194/bg-18-3579-2021

Reimer, P. J., Austin, W. E., Bard, E., Bayliss, A., Blackwell, P. G., Ramsey, C. B., et al. (2020). The IntCal20 Northern Hemisphere radiocarbon age calibration curve (0–55 cal kBP). *Radiocarbon*, *62*(4), 725–757. https://doi.org/10.1017/rdc.2020.41

Richter, N., Longo, W. M., George, S., Shipunova, A., Huang, Y., & Amaral-Zettler, L. (2019). Phylogenetic diversity in freshwater-dwelling Isochrysidales haptophytes with implications for alkenone production. *Geobiology*, *17*(3), 272–280. https://doi.org/10.1111/gbi.12330

Richter, N., Russell, J. M., Garfinkel, J., & Huang, Y. (2021). Winter–spring warming in the North Atlantic during the last 2000 years: Evidence from southwest Iceland. *Climate of the Past*, *17*(3), 1363–1383. https://doi.org/10.5194/cp-17-1363-2021

Russell, J. M., Hopmans, E. C., Loomis, S. E., Liang, J., & Sinninghe Damsté, J. S. (2018). Distributions of 5- and 6-methyl branched glycerol dialkyl glycerol tetraethers (brGDGTs) in East African lake sediment: Effects of temperature, pH, and new lacustrine paleotemperature calibrations. *Organic Geochemistry*, *117*, 56–69. https://doi.org/10.1016/j.orggeochem.2017.12.003

Saros, J. E., Anderson, N. J., Juggins, S., McGowan, S., Yde, J. C., Telling, J., et al. (2019). Arctic climate shifts drive rapid ecosystem responses across the West Greenland landscape. *Environmental Research Letters*, *14*(7), 074027. https://doi.org/10.1088/1748-9326/ab2928

Schouten, S., Hopmans, E. C., & Sinninghe Damsté, J. S. (2013). The organic geochemistry of glycerol dialkyl glycerol tetraether lipids: A review. *Organic Geochemistry*, *54*, 19–61. https://doi.org/10.1016/j.orggeochem.2012.09.006

Schweinsberg, A. D., Briner, J. P., Licciardi, J. M., Bennike, O., Lifton, N. A., Graham, B. L., et al. (2019). Multiple independent records of local glacier variability on Nuussuaq, West Greenland, during the Holocene. *Quaternary Science Reviews*, *215*, 253–271. https://doi.org/10.1016/j.quascirev.2019.05.007

Schweinsberg, A. D., Briner, J. P., Miller, G. H., Bennike, O., & Thomas, E. K. (2017). Local glaciation in West Greenland linked to North Atlantic Ocean circulation during the Holocene. *Geology*, *45*(3), 195–198. https://doi.org/10.1130/G38114.1

Shanahan, T. M., Hughen, K. A., & Van Mooy, B. A. S. (2013). Temperature sensitivity of branched and isoprenoid GDGTs in Arctic lakes. *Organic Geochemistry*, *64*, 119–128. https://doi.org/10.1016/j.orggeochem.2013.09.010

Sinninghe Damsté, J. S., Rijpstra, W. I. C., Foesel, B. U., Huber, K. J., Overmann, J., Nakagawa, S., et al. (2018). An overview of the occurrence of ether-and ester-linked iso-diabolic acid membrane lipids in microbial cultures of the Acidobacteria: Implications for brGDGT paleoproxies for temperature and pH. *Organic Geochemistry*, *124*, 63–76. https://doi.org/10.1016/j.orggeochem.2018.07.006

Sinninghe Damsté, J. S., Weber, Y., Zopfi, J., Lehmann, M. F., & Niemann, H. (2022). Distributions and sources of isoprenoidal GDGTs in Lake Lugano and other central European (peri-)alpine lakes: Lessons for their use as paleotemperature proxies. *Quaternary Science Reviews*, *277*, 107352. https://doi.org/10.1016/j.quascirev.2021.107352

Šmejkalová, T., Edwards, M. E., & Dash, J. (2016). Arctic lakes show strong decadal trend in earlier spring ice-out. *Scientific Reports*, *6*(1), 38449. https://doi.org/10.1038/srep38449

Smol, J. P., Wolfe, A. P., Birks, H. J. B., Douglas, M. S., Jones, V. J., Korhola, A., et al. (2005). Climate-driven regime shifts in the biological communities of arctic lakes. *Proceedings of the National Academy of Sciences of the United States of America*, *102*(12), 4397–4402. https://doi.org/10.1073/pnas.0500245102

Stahl, D. A., & de la Torre, J. R. (2012). Physiology and diversity of ammonia-oxidizing archaea. *Annual Review of Microbiology*, *66*(1), 83–101. https://doi.org/10.1146/annurev-micro-092611-150128

Stefanescu, I. C., Shuman, B. N., & Tierney, J. E. (2021). Temperature and water depth effects on brGDGT distributions in sub-alpine lakes of mid-latitude North America. *Organic Geochemistry*, *152*, 104174. https://doi.org/10.1016/j.orggeochem.2020.104174

Sun, Q., Chu, G., Liu, M., Xie, M., Li, S., Ling, Y., et al. (2011). Distributions and temperature dependence of branched glycerol dialkyl glycerol tetraethers in recent lacustrine sediments from China and Nepal. *Journal of Geophysical Research*, *116*(G1), G01008. https://doi.org/10.1029/2010jg001365

Tierney, J. E., & Russell, J. M. (2009). Distributions of branched GDGTs in a tropical lake system: Implications for lacustrine application of the MBT/CBT paleoproxy. *Organic Geochemistry*, *40*(9), 1032–1036. https://doi.org/10.1016/j.orggeochem.2009.04.014

Theroux, S., D'Andrea, W. J., Toney, J., Amaral-Zettler, L., & Huang, Y. (2010). Phylogenetic diversity and evolutionary relatedness of alkenone-producing haptophyte algae in lakes: Implications for continental paleotemperature reconstructions. *Earth and Planetary Science Letters*, *300*(3–4), 311–320. https://doi.org/10.1016/j.epsl.2010.10.009

Theroux, S., Huang, Y., & Amaral-Zettler, L. (2012). Comparative molecular microbial ecology of the spring haptophyte bloom in a Greenland Arctic oligosaline lake. *Frontiers in Microbiology*, *3*, 415. https://doi.org/10.3389/fmicb.2012.00415

Theroux, S., Huang, Y., Toney, J. L., Andersen, R., Nyren, P., Bohn, R., et al. (2020). Successional blooms of alkenone-producing haptophytes in Lake George, North Dakota: Implications for continental paleoclimate reconstructions. *Limnology and Oceanography*, *65*(2), 413–425. https://doi.org/10.1002/lno.11311

Thomas, E. K., Castañeda, I. S., McKay, N. P., Briner, J. P., Salacup, J. M., Nguyen, K. Q., & Schweinsberg, A. D. (2018). A wetter Arctic coincident with hemispheric warming 8,000 years ago. *Geophysical Research Letters*, *45*(19), 10637–10647. https://doi.org/10.1029/2018GL079517

Tomkins, J. D., Antoniades, D., Lamoureux, S. F., & Vincent, W. F. (2008). A simple and effective method for preserving the sediment–water interface of sediment cores during transport. *Journal of Paleolimnology*, *40*(1), 577–582. https://doi.org/10.1007/s10933-007-9175-1

van Bree, L. G. J., Peterse, F., Baxter, A. J., De Crop, W., van Grinsven, S., Villanueva, L., et al. (2020). Seasonal variability and sources of in situ brGDGT production in a permanently stratified African crater lake. *Biogeosciences*, *17*(21), 5443–5463. https://doi.org/10.5194/bg-17-5443-2020

van der Bilt, W. G. M., D'Andrea, W. J., Bakke, J., Balascio, N. L., Werner, J. P., Gjerde, M., & Bradley, R. S. (2018). Alkenone-based reconstructions reveal four-phase Holocene temperature evolution for High Arctic Svalbard. *Quaternary Science Reviews*, *183*, 204–213. https://doi.org/10.1016/j.quascirev.2016.10.006

van der Bilt, W. G. M., D'Andrea, W. J., Werner, J. P., & Bakke, J. (2019). Early Holocene temperature oscillations exceed amplitude of observed and projected warming in Svalbard lakes. *Geophysical Research Letters*, *46*(24), 14732–14741. https://doi.org/10.1029/2019GL084384

Weber, Y., Sinninghe Damsté, J. S., Zopfi, J., De Jonge, C., Gilli, A., Schubert, C. J., et al. (2018). Redox-dependent niche differentiation provides evidence for multiple bacterial sources of glycerol tetraether lipids in lakes. *Proceedings of the National Academy of Sciences of the United States of America*, *115*(43), 10926–10931. https://doi.org/10.1073/pnas.1805186115

Weijers, J. W. H., Schouten, S., van den Donker, J. C., Hopmans, E. C., & Sinninghe Damsté, J. S. (2007). Environmental controls on bacterial tetraether membrane lipid distribution in soils. *Geochimica et Cosmochimica Acta*, *71*(3), 703–713. https://doi.org/10.1016/j.gca.2006.10.003

Weiser, J., Titschack, J., Kienast, M., McCave, I. N., Lochte, A. A., Saini, J., et al. (2021). Atlantic water inflow to Labrador Sea and its interaction with ice sheet dynamics during the Holocene. *Quaternary Science Reviews*, *256*, 106833. https://doi.org/10.1016/j.quascirev.2021.106833

Woelders, L., Lenaerts, J. T., Hagemans, K., Akkerman, K., van Hoof, T. B., & Hoek, W. Z. (2018). Recent climate warming drives ecological change in a remote high-Arctic lake. *Scientific Reports*, *8*(1), 1–8. https://doi.org/10.1038/s41598-018-25148-7

Woolway, R. I., Kraemer, B. M., Lenters, J. D., Merchant, C. J., O'Reilly, C. M., & Sharma, S. (2020). Global lake responses to climate change. *Nature Reviews Earth & Environment*, *1*(8), 388–403. https://doi.org/10.1038/s43017-020-0067-5

Wu, J., Yang, H., Pancost, R. D., Naafs, B. D. A., Qian, S., Dang, X., et al. (2021). Variations in dissolved O_2 in a Chinese lake drive changes in microbial communities and impact sedimentary GDGT distributions. *Chemical Geology*, *579*, 120348. https://doi.org/10.1016/j.chemgeo.2021.120348

Yao, Y., Zhao, J., Vachula, R. S., Werne, J. P., Wu, J., Song, X., & Huang, Y. (2020). Correlation between the ratio of 5-methyl hexamethylated to pentamethylated branched GDGTs (HP5) and water depth reflects redox variations in stratified lakes. *Organic Geochemistry*, *147*, 104076. https://doi.org/10.1016/j.orggeochem.2020.104076

Young, N. E., Briner, J. P., Miller, G. H., Lesnek, A. J., Crump, S. E., Thomas, E. K., et al. (2020). Deglaciation of the Greenland and Laurentide ice sheets interrupted by glacier advance during abrupt coolings. *Quaternary Science Reviews*, *229*, 106091. https://doi.org/10.1016/j.quascirev.2019.106091

Zhang, Y. G., Zhang, C. L., Liu, X.-L., Li, L., Hinrichs, K.-U., & Noakes, J. E. (2011). Methane index: A tetraether archaeal lipid biomarker indicator for detecting the instability of marine gas hydrates. *Earth and Planetary Science Letters*, *307*(3–4), 525–534. https://doi.org/10.1016/j.epsl.2011.05.031

Zhang, Z., Smittenberg, R. H., & Bradley, R. S. (2016). GDGT distribution in a stratified lake and implications for the application of TEX86 in paleoenvironmental reconstructions. *Scientific Reports*, *6*(1), 34465. https://doi.org/10.1038/srep34465

Zhao, B., Castañeda, I. S., Bradley, R. S., Salacup, J. M., de Wet, G. A., Daniels, W. C., & Schneider, T. (2021). Development of an in situ branched GDGT calibration in Lake 578, southern Greenland. *Organic Geochemistry*, *152*, 104168. https://doi.org/10.1016/j.orggeochem.2020.104168

References From the Supporting Information

Hopmans, E. C., Schouten, S., & Damsté, J. S. S. (2016). The effect of improved chromatography on GDGT-based palaeoproxies. *Organic Geochemistry*, *93*, 1–6. https://doi.org/10.1016/j.orggeochem.2015.12.006

Huguet, C., Hopmans, E. C., Febo-Ayala, W., Thompson, D. H., Damsté, J. S. S., & Schouten, S. (2006). An improved method to determine the absolute abundance of glycerol dibiphytanyl glycerol tetraether lipids. *Organic Geochemistry*, *37*(9), 1036–1041. https://doi.org/10.1016/j.orggeochem.2006.05.008

Longo, W. M., Dillon, J. T., Tarozo, R., Salacup, J. M., & Huang, Y. (2013). Unprecedented separation of long chain alkenones from gas chromatography with a poly(trifluoropropylmethylsiloxane) stationary phase. *Organic Geochemistry*, *65*, 94–102. https://doi.org/10.1016/j.orggeochem.2013.10.011

Michelutti, N., Blais, J. M., Cumming, B. F., Paterson, A. M., Rühland, K., Wolfe, A. P., & Smol, J. P. (2010). Do spectrally inferred determinations of chlorophyll a reflect trends in lake trophic status? *Journal of Paleolimnology*, *43*(2), 205–217. https://doi.org/10.1007/s10933-009-9325-8